Cell

Resource

Cerebrospinal fluid immune dysregulation during healthy brain aging and cognitive impairment

Graphical abstract

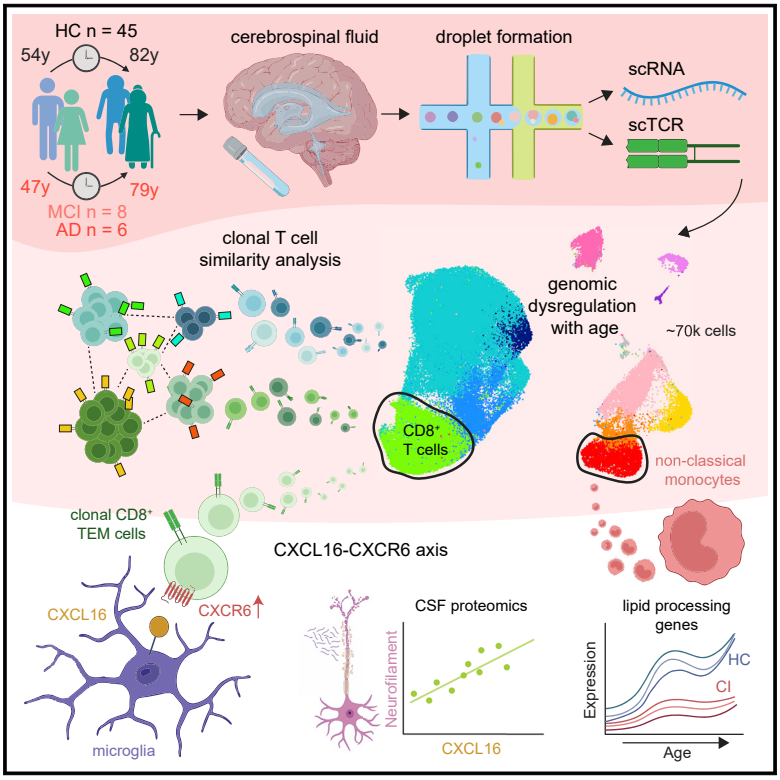

Highlights

- Monocytes upregulate lipid processing genes with age in cognitively normal CSF
- Monocyte lipid processing genes are dysregulated in cognitively impaired CSF
- Monocytes signal to clonal CD8$^+$ T cells via CXCL16-CXCR6 in cognitively impaired CSF
- CXCL16 is increased in cognitively impaired CSF and relates to neurodegeneration

Authors

Natalie Piehl, Lynn van Olst, Abhirami Ramakrishnan, ..., Anthony D. Wagner, Tony Wyss-Coray, David Gate

Correspondence

dgate@northwestern.edu

In brief

A single-cell transcriptomic resource exploring the cerebrospinal fluid immune system in healthy brain aging and cognitive impairment uncovers the CXCL16-CXCR6 pathway as a mediator of CD8$^+$ T cell trafficking to the CSF.

Piehl et al., 2022, Cell *185*, 5028–5039
December 22, 2022
https://doi.org/10.1016/j.cell.2022.11.019

CellPress

CellPress
OPEN ACCESS

Cell

Resource

Cerebrospinal fluid immune dysregulation during healthy brain aging and cognitive impairment

Natalie Piehl,[1] Lynn van Olst,[1] Abhirami Ramakrishnan,[1] Victoria Teregulova,[1] Brooke Simonton,[1] Ziyang Zhang,[1] Emma Tapp,[2] Divya Channappa,[2] Hamilton Oh,[3,4,5] Patricia M. Losada,[2,3] Jarod Rutledge,[3,4,6] Alexandra N. Trelle,[7] Elizabeth C. Mormino,[3,7] Fanny Elahi,[8] Douglas R. Galasko,[9] Victor W. Henderson,[2] Anthony D. Wagner,[3,7] Tony Wyss-Coray,[2,3,4,10,11] and David Gate[1,12,*]

[1]The Ken & Ruth Davee Department of Neurology, Northwestern University Feinberg School of Medicine, Chicago, IL, USA
[2]Department of Neurology and Neurological Sciences, Stanford University School of Medicine, Stanford, CA, USA
[3]Wu Tsai Neurosciences Institute, Stanford University, Stanford, CA, USA
[4]Paul F. Glenn Center for the Biology of Aging, Stanford University School of Medicine, Stanford, CA, USA
[5]Graduate Program in Stem Cell and Regenerative Medicine, Stanford University, Stanford, CA, USA
[6]Department of Genetics, Stanford University, Stanford, CA, USA
[7]Department of Psychology, Stanford University, Stanford, CA, USA
[8]Departments of Neurology and Neuroscience, Friedman Brain Institute, Icahn School of Medicine at Mount Sinai, La Jolla, CA, USA
[9]Department of Neurosciences, University of California at San Diego, La Jolla, CA, USA
[10]The Phil and Penny Initiative for Brain Resilience, Stanford University, Stanford, CA, USA
[11]Chemistry, Engineering, and Medicine for Human Health (ChEM-H), Stanford University, Stanford, CA, USA
[12]Lead contact
*Correspondence: dgate@northwestern.edu
https://doi.org/10.1016/j.cell.2022.11.019

SUMMARY

Cerebrospinal fluid (CSF) contains a tightly regulated immune system. However, knowledge is lacking about how CSF immunity is altered with aging or neurodegenerative disease. Here, we performed single-cell RNA sequencing on CSF from 45 cognitively normal subjects ranging from 54 to 82 years old. We uncovered an upregulation of lipid transport genes in monocytes with age. We then compared this cohort with 14 cognitively impaired subjects. In cognitively impaired subjects, downregulation of lipid transport genes in monocytes occurred concomitantly with altered cytokine signaling to CD8 T cells. Clonal CD8 T effector memory cells upregulated C-X-C motif chemokine receptor 6 (*CXCR6*) in cognitively impaired subjects. The CXCR6 ligand, C-X-C motif chemokine ligand 16 (CXCL16), was elevated in the CSF of cognitively impaired subjects, suggesting CXCL16-CXCR6 signaling as a mechanism for antigen-specific T cell entry into the brain. Cumulatively, these results reveal cerebrospinal fluid immune dysregulation during healthy brain aging and cognitive impairment.

INTRODUCTION

Neuroinflammation is a pathological hallmark of age-related neurodegenerative disease.[1] The brain is surrounded by the meninges, a membranous covering that contains the cerebrospinal fluid (CSF). The meningeal lymphatic system carries fluid and immune cells from the CSF to the deep cervical lymph nodes, enabling peripheral immune cells to respond to brain antigens under pathological conditions.[2,3] Adaptive immune T cells that initially encounter antigen in the periphery can enter the CSF via the systemic circulation and patrol the intrathecal space.[4–7] The choroid plexus, which produces the CSF, serves as an interface between the brain and circulation and is a site of age-related chronic neuroinflammation in mice.[8,9] Recent studies indicate the CSF provides molecular cues to immune cells of the skull bone marrow to alter CSF myeloid populations in mice.[10–12] However, the influence of age on the molecular mechanisms regulating CSF immunity in humans is not clear. Moreover, whether changes to the CSF immune system relate to behavioral changes such as cognitive impairment (CI) remains unknown.

Our recent studies indicate that CSF immune changes reflect the pathobiological events of age-related neurodegenerative disorders such as Alzheimer's disease (AD)[13] and Lewy body dementia.[14] We thus hypothesized that comparing the CSF immune transcriptomes associated with healthy cognitive aging and CI would provide insights into the pathophysiology of age-related neuroinflammation in neurodegenerative disease. Our results reveal age-related CSF immune perturbations in cognitively normal subjects, underscored by altered expression of lipid transport genes. Further, we detected an upregulation of C-X-C motif chemokine receptor 6 (*CXCR6*) in clonally expanded $CD8^+$ T effector memory (T_{EM}) cells of cognitively impaired subjects. The CXCR6 ligand, C-X-C motif chemokine ligand 16 (CXCL16), is a pleiotropic protein that functions as a T cell

chemoattractant and scavenger receptor for oxidized lipoprotein. CXCL16 was elevated in CSF of cognitively impaired subjects and was associated with neuroaxonal damage. We localized CXCR6$^+$ T cells and CXCL16$^+$ myeloid cells to amyloid plaques in AD post-mortem brains. Therefore, our single-cell transcriptomics resource identified the CXCL16-CXCR6 signaling axis as a potential mechanism for T cell entry into brains with neurodegeneration. Finally, we uncover an unexpected level of significantly altered AD risk genes in CSF T cells of cognitively impaired subjects. Altogether, these findings highlight the utility of measuring CSF immune changes to identify disease-associated neuroinflammation in cognitively impaired individuals.

RESULTS

Assessing CSF immunity in healthy brain aging and cognitive impairment by scRNA-seq

We first established age-related CSF immune transcriptome changes that occur with healthy brain aging. Extant studies on CSF immunity have suffered from biases associated with small sample sizes and limitations of conventional methods such as flow cytometry.[15,16] To circumvent these issues, we utilized our established droplet-based single-cell RNA sequencing (scRNA-seq) method[13,14,17] (Figure 1A). We generated CSF immune system profiles of 45 cognitively normal subjects ranging from 54 to 82 years old. We then compared CSF immune transcriptomes of this healthy cognitive aging group with 14 age- and sex-matched patients with clinical diagnoses of AD or prodromal mild cognitive impairment (MCI) (Figures 1B, S1A, and S1B). Comparison of Montreal cognitive assessment (MoCA) scores confirmed reduced cognitive abilities in MCI and AD subjects (Figure 1C). We also measured CSF biomarkers, which revealed higher levels of tau phosphorylated at residue 181 (pTau181) in cognitively impaired subjects (Figure 1C). Demographics and CSF biomarker data for these subjects are presented in Table 1.

Overall, we analyzed 70,391 quality-controlled CSF immune cells. Importantly, we did not observe diagnostic differences by dimensionality reduction (Figure S1C). Further, quality control metrics indicated limited amounts of mitochondrial reads and expected numbers of counts and features per group (Figure S1C). We then removed low levels of ambient RNA contamination with SoupX[18] (Figures S1D and S1E). We resolved CSF immune cell types including CD4$^+$ and CD8$^+$ T cells, T regulatory cells (Tregs), natural killer (NK) cells, plasma cells, B cells, dendritic cells, and three populations of classical, intermediate, and non-classical monocytes distinguished by varying CD14 and CD16 expression and pseudotime analysis (Figures 1D and S1F). CSF immune clusters were annotated based on their expression of cardinal marker genes (Figure 1E). Number of counts and mitochondrial reads were also consistent per sample (Figure S1G). We did not observe overt changes in cell type composition with age (Figure S1H). Samples were processed on two separate days, but this did not introduce observable batch effects (Figure S1I). We quantified cell type frequency, which revealed the majority of CSF immune cells as CD4$^+$ and CD8$^+$ T cells (Figure 1F). Finally, our full dataset can be explored online using a data portal located at gatelabnu.shinyapps.io/csf_aging.

Linear CSF immune transcriptome changes associated with healthy brain aging

We began by assessing age-related transcriptomic changes to each cell type using linear regression. We noted that CD4$^+$ and CD8$^+$ T cells and non-classical monocytes had the most differentially expressed genes (DEGs) with age (Figure 1G; Table S1). Plotting DEGs with age revealed increased expression of cluster of differentiation 74 (*CD74*) among CD4$^+$ and CD8$^+$ T cells (Figure 1H). *CD74* encodes the human leukocyte antigen (HLA) class II histocompatibility antigen gamma chain, which is a marker of T cell activation.[19–22] CD4$^+$ and CD8$^+$ T cells also upregulated with age expression of genes encoding the granzyme family of serine proteases (Figure 1H; Table S1). Granzymes are released by cytotoxic T cells to induce apoptosis in the target cell.[23] Interestingly, non-classical monocytes exhibited a pronounced reduction in expression with age of cytokine genes such as C-C motif chemokine ligand 3 (*CCL3*), C-C motif chemokine ligand 4 (*CCL4*), tumor necrosis factor (*TNF*), and interleukin 1 beta (*IL1B*). This reduction in cytokine gene expression was accompanied by increased expression of genes involved in lipid transport, including apolipoprotein E (*APOE*), apolipoprotein C1 (*APOC1*), and phospholipid transfer protein (*PLTP*) (Figure 1H). Notably, mutations in *APOE* and *APOC1* are associated risk factors for AD.[24–30] Further, the *PLTP* gene encodes a key determinant of lipoprotein metabolism involved in regulating inflammation, including by modulating adaptive immune functions through alternation of T cell polarization.[31] Thus, linear modeling (LM) revealed age-related changes to the CSF immune system. These changes were underscored by altered expression of genes involved in lipoprotein metabolism that are also established genetic risk factors for age-related neurodegeneration.

Non-linear CSF immune transcriptome changes associated with healthy brain aging

When visualizing gene expression with age, we noted that CSF immune genes fluctuated in distinct, non-linear patterns. We thus sought to visualize non-linear changes to CSF immune genes and to compare gene expression trajectories of CSF immune cells with age. Plotting expression of the 7,980 genes detected in non-classical monocytes with age by locally estimated scatterplot smoothing (LOESS) revealed wave-like expression trajectories (Figure 2A). We used hierarchical clustering to identify distinct patterns of gene expression changes with age (Figures 2B and S2; Table S1). To further validate gene expression changes with age, we divided healthy control (HC) subjects into middle (<70 years) and advanced ($\geq$70 years) age groups using the median age of 70 years old as a cutoff. We then performed differential expression (DE) by model-based analysis of single-cell transcriptomics (MAST)[32] (Figures 2C and S3B; Table S2). Importantly, we did not observe major effects of sex on the CSF immune transcriptome by MAST DE (Figure S3A; Table S2). However, DE of advanced and middle-aged groups also showed the highest level of immune dysregulation in non-classical monocytes (Figure 2C; Table S2). We then plotted upregulated genes of non-classical monocytes by LOESS, which

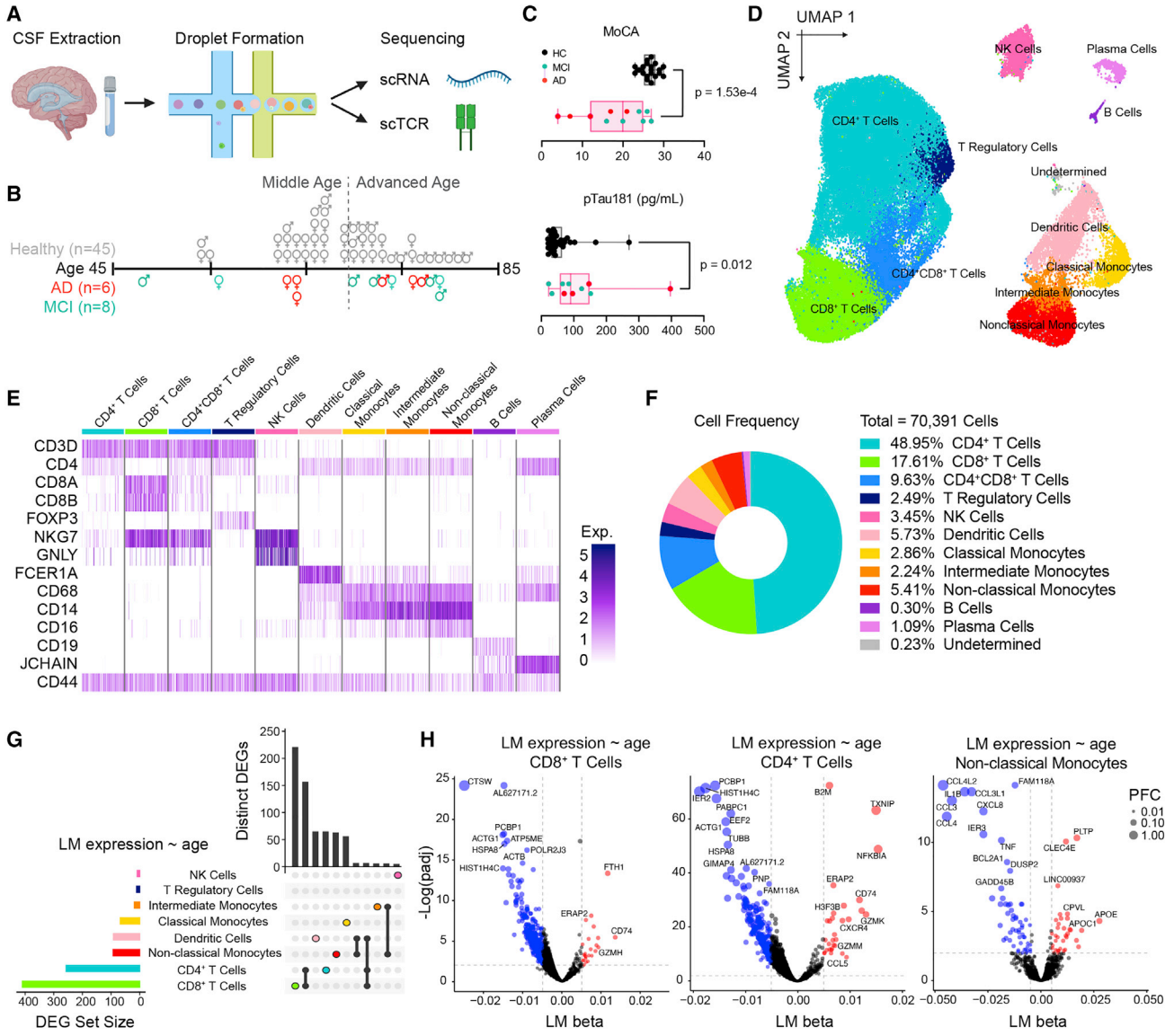

Figure 1. Study design and CSF immune cell gene expression changes by linear modeling

(A) Schematic depicting study design. CSF was isolated by lumbar puncture from living individuals. Single cells were loaded into droplets; then, libraries were amplified for whole transcriptome or targeted TCR sequencing.

(B) Study demographics indicating age and sex of each individual.

(C) MoCA cognitive scores and pTau181 levels in control vs. cognitively impaired subjects. Mean ± SEM; Mann-Whitney U test.

(D) UMAP plot showing clusters of CSF immune cells.

(E) Heatmap of marker genes utilized to annotate cell clusters.

(F) Donut plot indicating the distribution of CSF immune cell types.

(G) UpSet plot showing the number of DEGs per CSF immune cell cluster.

(H) Volcano plots depicting DEGs of the most altered clusters by linear modeling (LM).

See also Figure S1 and Table S1.

confirmed increased, non-linear expression of lipid transport genes *APOE*, *APOC1*, and *PLTP* with age (Figure 2D). Thus, our non-linear analysis uncovered changes to lipid processing genes of non-classical monocytes that dovetailed with our linear analysis.

We next sought to measure the age at which most gene expression changes were occurring. To measure non-linear gene expression changes, we used the algorithm DE-sliding window analysis (DE-SWAN).[33] We used DE-SWAN to analyze gene levels within a window of 4 years by comparing groups in parcels of 2 years (e.g., 60–62 years compared with 62–64 years), then sliding the window in increments of 2 years from youngest to oldest (Figure 2E). Using DE-SWAN, we detected a peak of DE for several CSF immune clusters at age 78 (Figure 2F; Table S3).

Table 1. Demographics and biomarker data of study subjects

		Healthy controls	Cognitively impaired	p value
Demographics				
Cognitive impairment, n (%)	HC	45 (100.0%)	0 (0.0%)	<0.001
	MCI	0 (0.0%)	8 (57.1%)	–
	AD	0 (0.0%)	6 (42.9%)	–
Sex, n (%)	female	27 (60.0%)	7 (50.0%)	0.725
	male	18 (40.0%)	7 (50.0%)	–
Age	median (interquartile range [IQR])	69.0 (65.0 to 73.0)	72.5 (64.0 to 76.8)	0.475
Race, n (%)	Asian	3 (6.7%)	1 (7.1%)	0.565
	Native Hawaiian or Other Pacific Islander	1 (2.2%)	–	–
	White	35 (77.8%)	9 (64.3%)	–
	N/A	6 (13.3%)	4 (28.6%)	–
APOE genotype		n = 38	n = 10	
	E3/E2	4 (10.5%)	1 (10.0%)	0.360
	E3/E3	16 (42.1%)	2 (20.0%)	
	E3/E4	16 (42.1%)	5 (50.0%)	
	E4/E4	2 (5.3%)	2 (20.0%)	
MoCA score		n = 22	n = 12	
	median (IQR)	27.0 (26.0–28.0)	20.5 (15.0–24.2)	<0.001
CDR		n = 42	n = 11	
	median (IQR)	0.0 (0.0–0.0)	1.0 (1.0–3.2)	<0.001
CSF biomarkers (pg/mL)		n = 37	n = 10	
pTau181	median (IQR)	40.1 (32.9–61.2)	91.1 (67.2–141.8)	0.012
Total tau	median (IQR)	302.0 (265.0–412.3)	604.6 (453.3–819.7)	0.006
Aβ42	median (IQR)	1,000.0 (811.3–1,231.3)	870.1 (673.8–1,014.8)	0.311
Aβ40	median (IQR)	10,565.0 (8,816.0–12,383.0)	12,061.5 (9,888.0–13,718.5)	0.203
CSF biomarker ratios		n = 37	n = 10	
Aβ42/Aβ40	median (IQR)	0.115 (0.078–0.126)	0.073 (0.063–0.115)	0.264
Aβ42/total tau	median (IQR)	3.900 (2.033–4.577)	1.247 (1.036–2.611)	0.015

Comparing DEGs by DE-SWAN and LM underscored the effects of advanced age on non-classical monocytes (Figure 2G). We then plotted genes of each cluster by the significance of their DE at age 78, which revealed a large set of changing genes of Tregs and non-classical monocytes (Figures 2H and S3C; Table S3). Notably, we detected dysregulated progranulin (*GRN*) expression in non-classical monocytes at age 78 (Figure 2H). Mutations in *GRN* are associated with AD[34] and frontotemporal dementia.[35–37] Intriguingly, *GRN* encodes a key regulator of lysosomal function[38] and lipid accumulation in brain microglia.[39] Lipid processing genes were also altered in non-classical monocytes at age 78, including *APOC2* and apolipoprotein B receptor (*APOBR*) (Figure 2H).

Non-classical monocytes communicate with CD8$^+$ T cells via CXCL16-CXCR6 in cognitively impaired CSF

Having established gene expression patterns of CSF immune cells in healthy aging, we next aimed to compare these changes with subjects with CI. To our surprise, MAST DE of cognitively impaired vs. cognitively normal controls revealed the highest level of transcriptomic dysregulation in Tregs (Figure S4A; Table S4). Analysis of individual DEGs showed upregulated expression of forkhead box P3 (*FOXP3*) and interleukin 32 (*IL32*) in Tregs (Figure S4B; Table S4). Populations of classical and non-classical monocytes were also highly dysregulated (Figure S4A). Interestingly, we noted downregulated expression of *APOC1* in non-classical monocytes (Figure S4B). This prompted us to plot the expression of lipid processing genes of non-classical monocytes from cognitively impaired vs. cognitively normal subjects with age. Plotting *APOE*, *APOC1*, and *PLTP* with age by LOESS demonstrated reduced expression of all three genes in cognitively impaired subjects at later ages (Figure 2I). We thus performed MAST DE on non-classical monocytes comparing advanced age cognitively impaired subjects with advanced age cognitively normal subjects (Figures S3D and S3E). By this method, *APOE* and *APOC1* were highly downregulated, verifying reduced expression of lipid processing genes in cognitively impaired subjects with age (Figure 2J; Table S4).

We next aimed to determine whether reduced lipid processing gene expression among non-classical monocytes coincided with altered intercellular communication in the CSF. To infer cell-cell communication, we utilized CellChat. CellChat uses a signaling molecule interaction database of ligand-receptor interactions to analyze intercellular communications from

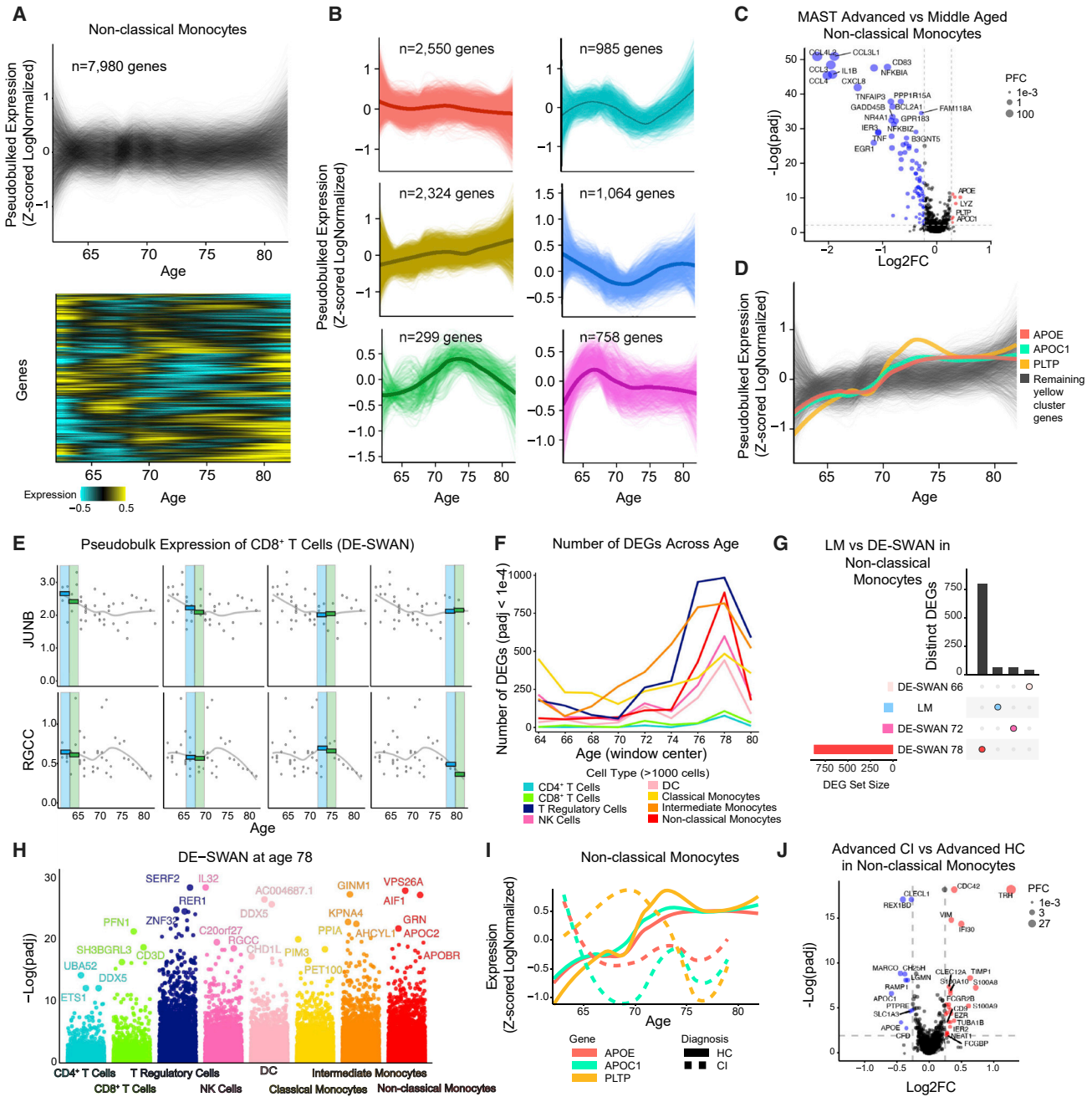

Figure 2. Upregulated lipid processing gene expression in non-classical CSF monocytes with age

(A) LOESS trajectories (upper) and a corresponding heatmap (lower) demonstrating wave-like expression patterns of non-classical monocytes with age.

(B) Sets of genes ordered by hierarchical clustering and displayed using LOESS trajectories display distinct wave-like patterns with age.

(C) Volcano plot from MAST differential expression analysis showing downregulation of cytokine genes and upregulation of lipid processing genes.

(D) LOESS trajectories of *APOE*, *APOC1*, and *PLTP* expression in non-classical CSF monocytes with age.

(E) Representative genes *JUNB* and *RGCC* display distinct non-linear changes with age. DE-SWAN was used to measure the age at which most differential expression occurs.

(F) The results of DE-SWAN analysis indicating a consistent dysregulation of CSF immune cell types at age 78.

(G) UpSet plot comparing the number of DEGs for non-classical CSF monocytes from DE-SWAN and linear modeling.

(H) Manhattan plot indicating genes that were differentially expressed by each cluster at age 78.

(I) LOESS trajectories of lipid processing genes comparing HC to CI subjects.

(J) Volcano plot showing reduction of lipid processing genes *APOE* and *APOC1* comparing only advanced aged subjects.

See also Figures S2 and S3 and Tables S1, S2, S3, and S4.

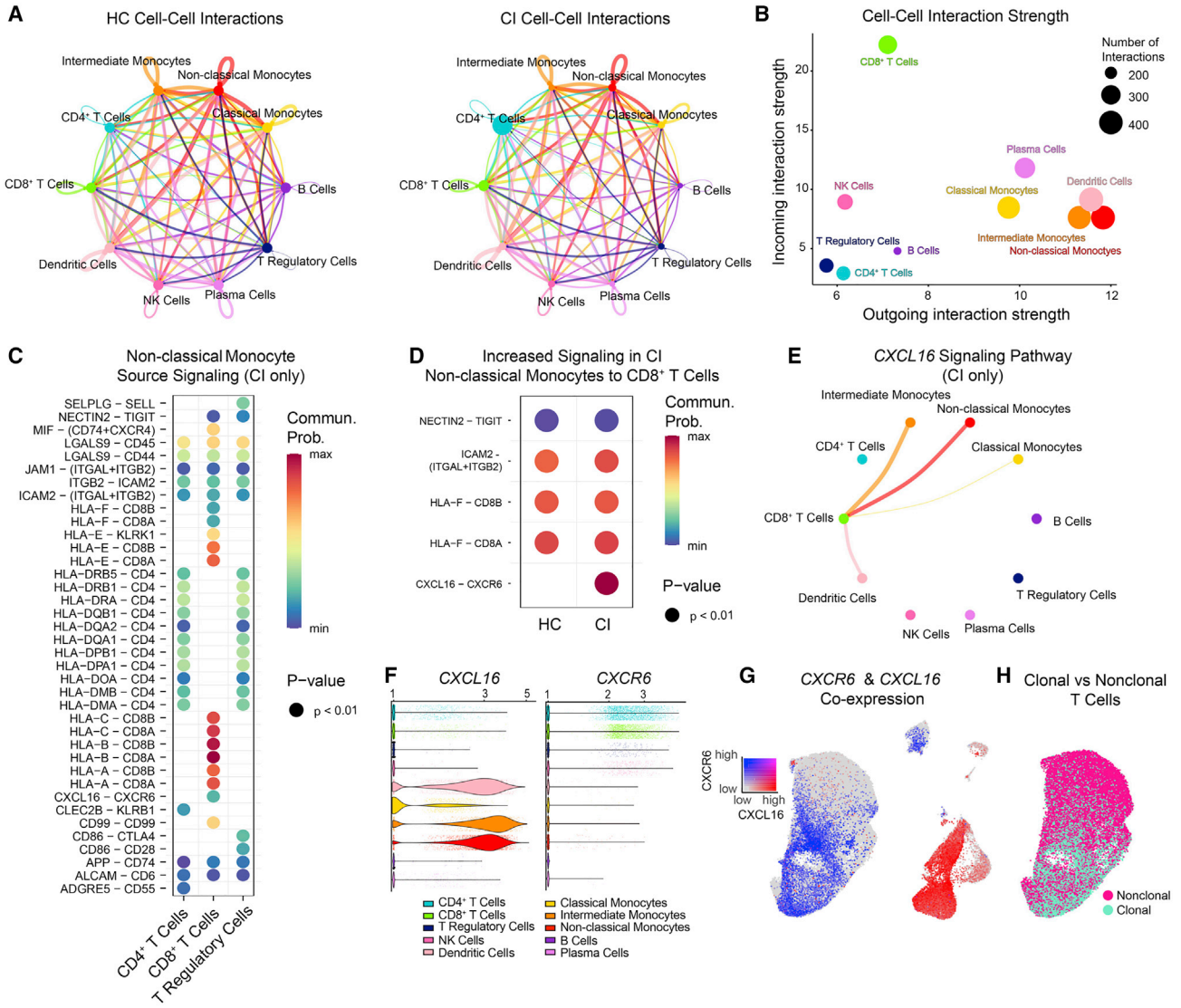

Figure 3. Cell-cell communication algorithm indicates non-classical monocytes communicate with CD8$^+$ T cells via CXCL16-CXCR6 signaling in cognitive impaired CSF

(A) Circle plots of signaling networks of healthy and cognitively impaired CSF immune systems.

(B) Cell-cell interaction strengths plotted for all cell types indicating incoming and outgoing interactions.

(C) Dot plot indicating signaling molecules between non-classical monocytes and T cells in cognitively impaired CSF.

(D) CXCL16-CXCR6 signaling between non-classical monocytes and CD8$^+$ T cells is unique to cognitively impaired CSF.

(E) The signaling network for CXCL16-CXCL6 indicates activated monocytes as the primary source of CXCL16 for CXCR6 on CD8$^+$ T cells.

(F) Violin plots indicating which cell types express CXCR6 and CXCL16 in the CSF.

(G) UMAP showing expression of CXCR6 by T cells and CXCL16 by myeloid cells.

(H) Distribution of clonal and nonclonal CSF T cells.

See also Figure S2.

scRNA-seq data.[40] Within our scRNA-seq data, cell-cell interactions of cognitively normal and cognitively impaired CSF appeared highly similar (Figure 3A). We detected the strongest incoming interactions among CD8$^+$ T cells and the strongest outgoing interactions coming from non-classical monocytes (Figure 3B). We then probed the cell-cell interactions of cognitively impaired CSF, which indicated strong communication probabilities between non-classical monocytes and CD8$^+$ T cells via HLA-A, HLA-B, HLA-C, and HLA-E binding CD8A and CD8B (Figure 3C). In fact, most signaling pairs between non-classical monocytes and CD8$^+$ T cells that were increased in cognitively impaired CSF were also increased in cognitively normal CSF. However, signaling between CXCL16 and CXCR6 was unique to cognitively impaired CSF (Figure 3D). Notably, CXCR6 is a surface chemokine receptor that regulates T cell migration to various tissues.[41] We then plotted the cell-cell interactions of

CXCL16-CXCR6 signaling in cognitively impaired CSF, which indicated non-classical monocytes as the primary source of CXCL16 for CXCR6 expressed on CD8$^+$ T cells (Figure 3E). We measured *CXCL16* and *CXCR6* among CSF cell types, which indicated expression of *CXCL16* by myeloid cells and *CXCR6* by T cells (Figures 3F and 3G). We next sequenced CSF T cell receptors (TCRs) from the same cells as above and noted an association of *CXCR6* expression with clonal T cells (Figure 3H). Altogether, these results show that myeloid cells communicate with clonal CD8$^+$ T cells via CXCL16-CXCR6 in cognitively impaired CSF. Interestingly, we also detected clonally expanded Tregs (Figure S4C), but these cells were too sparse to perform DE.

Dysregulation of clonally expanded CSF T cells of cognitively impaired subjects

We previously showed that clonally expanded T cells patrol the CSF in AD.[14] However, the mechanism by which antigen-specific T cells enter the CSF remains poorly understood. We therefore assessed the transcriptomes of clonally expanded T cells between cognitively impaired vs. cognitively normal CSF immune systems. We then asked whether CSF TCRs from cognitively impaired subjects were similar in protein sequence to those of cognitively normal subjects of advanced age. We used our established TCR Levenshtein similarity (Lsim) networking method[13,17,42] to compare TCRs of cognitively impaired patients with cognitively normal subjects of four equal-sized age bins (early and late middle age and early and late advanced age). These results showed increased similarity of TCRs from cognitively impaired subjects with the two oldest age bins (early and late advanced age) (Figure 4A; Table S4). Conversely, no similarities were detected between TCRs from cognitively impaired subjects with the two youngest age bins (Figures 4A and 4B; Table S4).

We next sought to determine whether clonally expanded, antigen-specific T cells were transcriptionally distinct in cognitively impaired vs. cognitively normal CSF immune systems. We thus performed DE on clonally expanded CD4$^+$ and CD8$^+$ T cells of cognitively impaired vs. cognitively normal CSF. MAST DE of nonclonal and clonal CD4$^+$ and CD8$^+$ T cells revealed T cell clonal expansion as a driver of transcriptional dysregulation in cognitively impaired vs. cognitively normal CSF (Figure 4C). We noted a shift from *CXCR4* to *CXCR6* chemokine receptor gene expression in clonally expanded CD4$^+$ and CD8$^+$ T cells (Figures S5A and S5B). Notably, clonally expanded CD8$^+$ T cells upregulated *CXCR6* in cognitively impaired vs. cognitively normal CSF (Figure 4D; Table S4). We further confirmed an increased *CXCR6* expression by CD8$^+$ T cells in cognitively impaired subjects on the pseudobulk level (Figure S5C).

We next aimed to obtain finer resolution of the CD8$^+$ T cell subtype associated with CI. To do so, we utilized a cellular indexing of transcriptomes and epitopes by sequencing (CITE-seq) reference dataset[43] and supervised clustering to reannotate the same CSF cells (Figures S5D and S5E). To our surprise, CD14$^+$ monocytes were the most dysregulated cell type among reannotated clusters (Figure S5F; Table S5). Having finer resolution of CSF immunity, we then measured *CXCR6* expression in T cell subsets, which distinguished CD8$^+$ and CD4$^+$ T_{EM} cells as the primary expressors of *CXCR6* (Figures 4F and S5G). We also observed increased *CXCR6* expression in CD8$^+$ T_{EM} cells on the pseudobulk level (Figure S5H). We then reassigned TCRs to these reannotated cells to identify clonal populations of CSF T cells (Figures 4G and S5I). We quantified single-cell expression of *CXCR6* on CD8 T_{EM} cells which revealed higher levels of expression among cognitively impaired subjects (Figure 4H).

Finally, we sought to measure levels of CSF CXCL16 protein in larger groups of subjects and to compare CXCL16 levels with neurodegenerative disease biomarkers. We first utilized a proximity extension assay (PEA), which detected higher levels of CXCL16 in CSF of cognitively impaired vs. cognitively normal subjects (Figures 4I and S6A). Notably, levels of CXCL16 highly correlated with levels of neurofilament light (NEFL) in cognitively impaired and cognitively normal subjects (Figure 4J; Table S6). NEFL is a biomarker for neuroaxonal damage which predicts neurodegeneration and clinical progression in presymptomatic AD.[44] CXCL16 also correlated with levels of CSF glial fibrillary acidic protein (GFAP) and ubiquitin C-terminal hydrolase L1 (UCHL1). Interestingly, CXCL16 did not correlate with either $A\beta_{40}$ or $A\beta_{42}$ but did correlate with pTau181 in subjects who were diagnosed with MCI and progressed to AD (Figure 4J). We confirmed our PEA results by detecting a positive correlation between CXCL16 and NEFL by slow off-rate modified aptamer (SOMAmer) assay (Figure 4K; Table S6). However, although the SOMAmer assay detected increased levels of CXCL16 in cognitively impaired subjects, we did not observe significant group differences (Figure S6B).

Interestingly, public datasets indicate that microglia/macrophages are the main expressors of *CXCL16* in human brain (Figure S6C).[45] Further, microglia express higher levels of *CXCL16* than monocytes (Figure S6D).[46] In AD brain, *CXCL16* is more highly expressed in the temporal cortex of AD subjects than controls (Figure S6E).[47] Thus, we aimed to confirm protein expression of CXCL16 in AD brain myeloid cells. Indeed, we identified CXCL16$^+$Iba1$^+$ plaque-associated myeloid cells in AD brain (Figure S6F). We confirmed intracellular expression of CXCL16 by Iba1$^+$ cells by generating a z stack through an Iba1$^+$ myeloid cell body (Figure S6G). Finally, we identified CD3$^+$ T cells expressing the CXCR6 receptor in close proximity to Iba1$^+$ myeloid cells in two separate AD post-mortem brains (Figure S6H). Cumulatively, these results indicate altered CXCR6-CXCL16 signaling as a mechanism for antigen-experienced T cell entry into the brains of subjects with neurodegeneration.

Our results uncover T cell transcriptomic changes associated with CI. Historically, innate immunity has been studied in greater detail than adaptive immunity in AD. The identification of AD risk genes via genome-wide association studies (GWASs)[48,49] further compelled AD researchers to interrogate brain innate immunity, since many AD risk genes are expressed by brain innate immune cells. However, when we probed AD risk genes for expression among CSF immune cells,[50] we identified CD4$^+$ and CD8$^+$ T cells as having the most significantly altered genes (Figure 5). Among supervised clusters, CD4$^+$ T_{EM} and CD8$^+$ T_{EM} cells had the most altered AD risk genes (Figure S6I). Altogether, these results uncover a potential, unexpected role of T cells in AD risk.

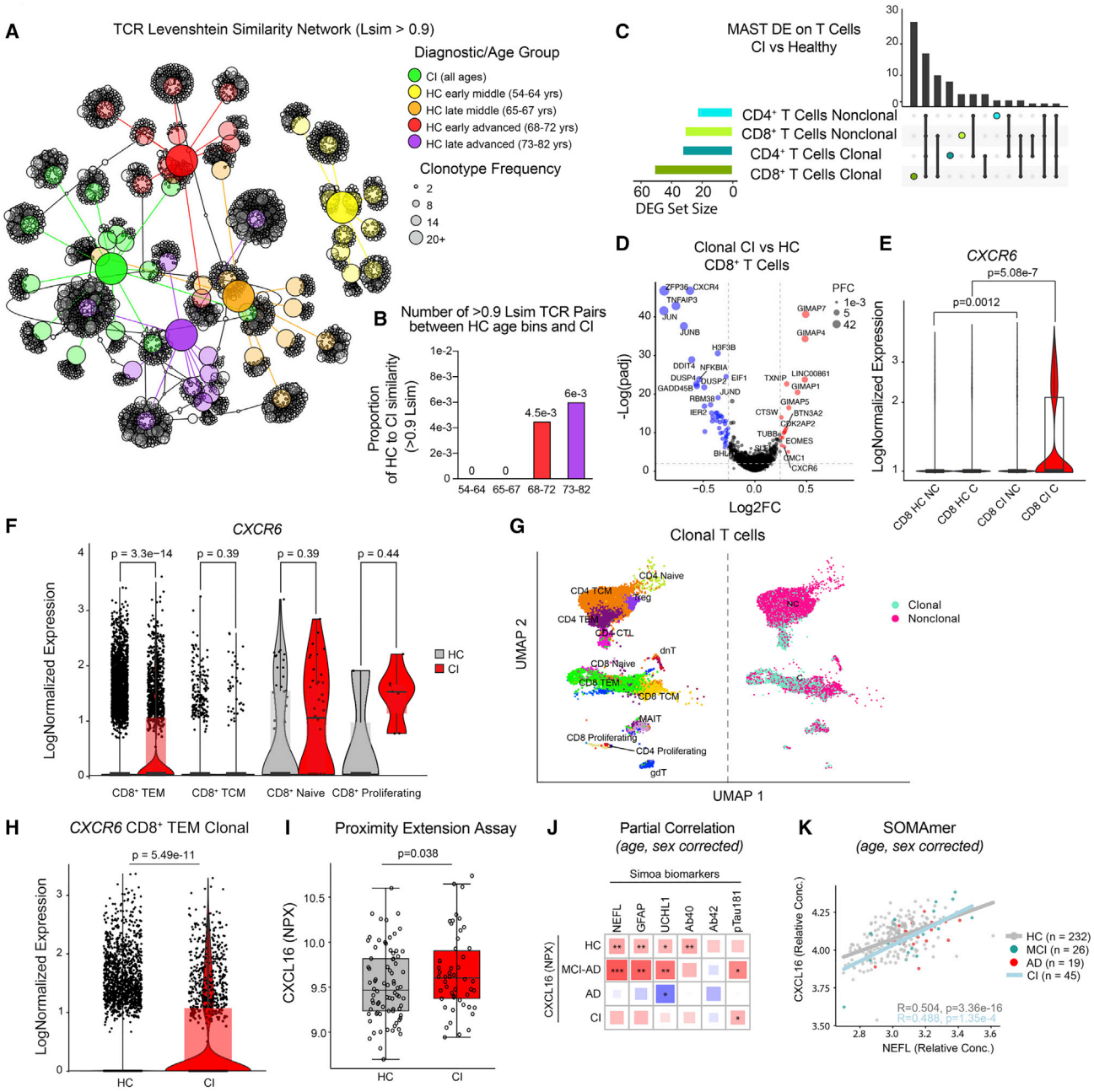

Figure 4. Clonally expanded T cell disruption in CSF of patients with cognitive impairment

(A) TCR networking plot depicting Levenshtein similarities >0.9 for all clonal CSF TCRs. Healthy, cognitively normal patients were binned into equal-sized groups.

(B) Quantification of the proportion of TCRs for each age group that had Levenshtein similarity >0.9.

(C) UpSet plot showing that clonally expanded $CD4^+$ and $CD8^+$ T cells have more DEGs that nonclonal T cells.

(D) Volcano plots showing DEGs of clonal vs. nonclonal $CD8^+$ T cells between cognitively impaired and healthy CSF.

(E) Quantification of average single-cell expression of clonal and nonclonal $CD8^+$ T cells from cognitively impaired and healthy CSF. p values are from MAST differential expression.

(F) Single-cell quantification of CXCR6 expression by $CD8^+$ T cell subtypes showing increased expression among $CD8^+$ T_{EM} cells. Wilcox test, BH corrected.

(G) UMAP showing distribution of T cell subtypes and clonality using supervised clustering.

(H) Single-cell quantification of *CXCR6* expression in clonal $CD8^+$ T_{EM} cells showing higher expression among cognitively impaired subjects. Wilcox test.

(I) PEA assay measurement of CXCL16 protein showing higher levels in cognitively impaired subjects. ANCOVA with sex and age as covariates. Error bars indicate upper or lower interquartile range (IQR) plus or minus 1.5*IQR.

(J) Correlations of CXCL16 with CSF biomarkers. Spearman partial correlation with sex and age as additional covariates.

(K) Correlations between CSF CXCL16 and NEFL using SOMAmer measurements. Spearman partial correlation with sex and age as additional covariates.

See also Figures S4, S5, and S6 and Tables S4, S5, and S6.

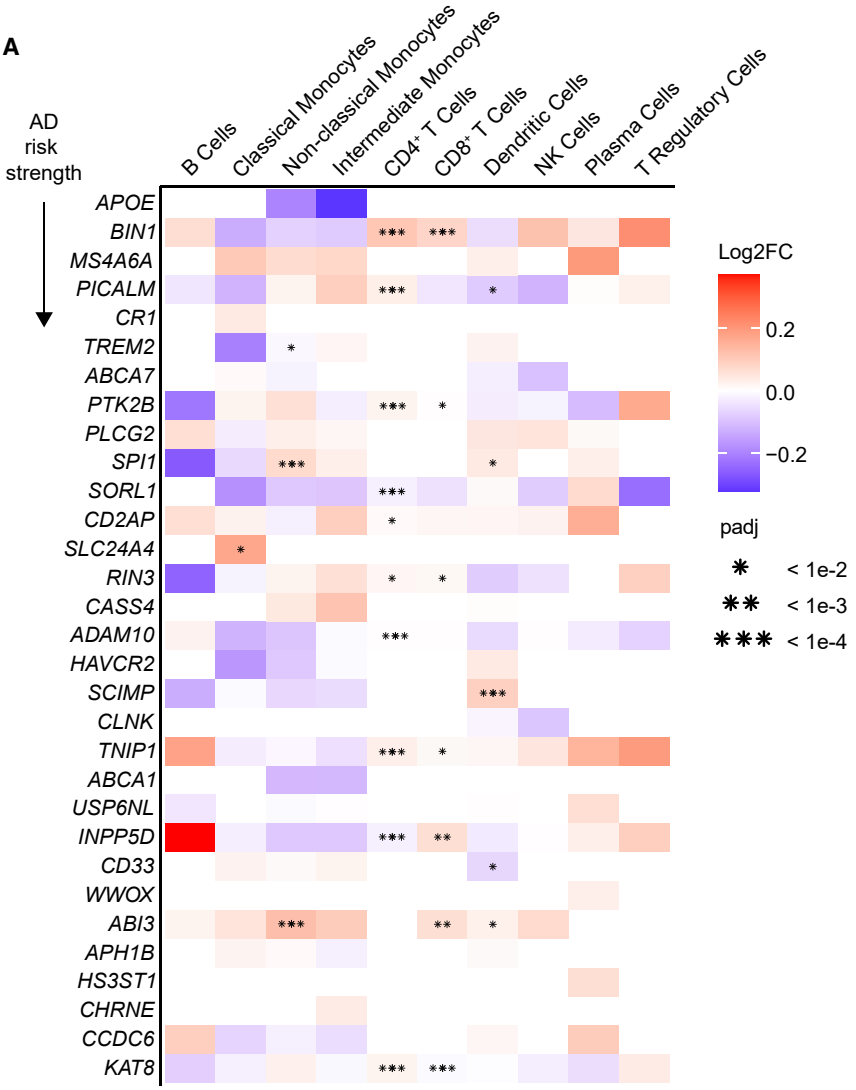

Figure 5. Differential expression of the top 45 AD GWAS genes across all major CSF immune cell types

Asterisks denote the most highly altered genes by adjusted p value. Note that T cells differentially express numerous AD risk genes in CI CSF.
See also Figure S6.

DISCUSSION

Our CSF immune transcriptomic profiling provides insight into the influence of age on healthy brain aging and into the pathophysiology of CI. In healthy brain aging, we identified a population of non-classical CSF monocytes with increased expression of genes encoding lipid processing proteins. Some of the genes associated with CSF monocyte aging are genetic risk factors for AD, including *APOE* and *APOC1*. Increased expression of these genes by intrathecal monocytes highlights the critical role of lipid metabolism in innate immunity and immunoregulation.[51] Particularly intriguing was the concomitant downregulation of cytokine genes, suggestive of a metabolic and functional shift of non-classical monocytes with age. These changes might reflect parenchymal myeloid cell pathophysiology, such as the accumulation of lipid droplets in brain microglia with age.[39]

Our results also indicate disparate age-related CSF immune system perturbations in cognitively impaired subjects. These transcriptional changes may reflect alterations to CSF immunity during the neurodegenerative disease course. Among significantly altered CSF immune cells were non-classical monocytes, which show decreased expression of lipid transport genes concomitant with increased signaling to $CD8^+$ T cells via CXCL16-CXCR6. Intriguingly, CXCL16 has a dual role as a scavenger receptor that mediates internalization of oxidized low-density lipoproteins.[52] Thus, increased CXCL16 in the CSF of cognitively impaired subjects may be compensatory to reduced lipid transport gene expression in non-classical monocytes. Additionally, CXCL16 is a receptor for phosphatidylserine-coated particles such as apoptotic bodies. Therefore, the correlation between CXLC16 and neuroaxonal damage may reflect the immune response to neuronal death.

Our results show that TCRs of cognitively impaired subjects more closely resemble those from advanced ages than younger age groups. This suggests that the TCR repertoire of cognitively impaired subjects resembles an "advanced aging" CSF adaptive immune system. Moreover, we identify an association between *CXCR6* expression in clonally expanded T cells and CI. Our results suggest that CXCR6 regulates homing of antigen-specific T cells from the peripheral circulation to the CSF via brain myeloid expression of CXCL16. This finding is particularly enlightening in conjunction with recent evidence that CXCR6/CXCL16 signaling functions as a maintenance factor for brain resident T cells that drive synapse elimination during viral recovery in mice.[53]

Altogether, our results highlight the potential to utilize CSF immune transcriptome changes to identify disease-associated neuroinflammation in cognitively impaired individuals. As such, CSF immunophenotyping may be useful to gain further insight into T cell-antigen complexes involved in the pathophysiology of CI. Here, we uncover CXCL16-CXCR6 signaling as a potential mechanism of antigen-specific T cell entry into the intrathecal space of patients with CI. These findings could be used to improve anti-inflammatory therapeutics or to estimate levels of neuroinflammation in cognitively impaired patients.

Limitations of the study

This study is comprised entirely of human data, and our claims are based primarily on bioinformatic approaches that rely on

underlying assumptions of algorithms. As such, there are limitations regarding functional or mechanistic evidence. Ideally, *in vivo* experiments in animals would further elucidate the necessity and sufficiency of CXCL16-CXCR6 signaling in T cell brain homing and its impact on cognition. We encourage animal researchers to interrogate this pathway. Additionally, females comprised most of the younger healthy controls, whereas males comprised most of the older healthy controls in this study. Thus, while we did not observe sex effects in this study, we suggest further interrogation of potential sex differences in CSF immunity.

STAR★METHODS

Detailed methods are provided in the online version of this paper and include the following:

- KEY RESOURCES TABLE
- RESOURCE AVAILABILITY
  - Lead Contact
  - Materials Availability
  - Data and Code Availability
- EXPERIMENTAL MODEL AND SUBJECT DETAILS
  - Human Subjects
- METHOD DETAILS
  - Sample Preparation
  - Protein biomarker measurements
  - Droplet-based scRNA and TCRseq
  - scRNA and TCRseq quality control
  - Cell type annotations
  - Differential expression by linear modelling
  - DE-SWAN analysis
  - LOESS trajectory analysis
  - Differential expression by MAST
  - CellChat analysis
  - Levenshtein similarity network
  - Clone expression scatterplot
  - Immunohistochemistry and confocal imaging
  - ShinyCell
- QUANTIFICATION AND STATISTICAL ANALYSIS

SUPPLEMENTAL INFORMATION

Supplemental information can be found online at https://doi.org/10.1016/j.cell.2022.11.019.

ACKNOWLEDGMENTS

We thank A.C. Yang (UC, San Francisco) and R.T. Vest (Qinotto Inc.) for helpful advice. We also thank the clinical staffs of the Stanford Alzheimer's Disease Research Center (ADRC) and the Stanford Brain Rejuvenation Program for their assistance acquiring patient samples. Some figures were created using BioRender.com. This work was supported by a NIA R01AG078713-01 (D.G.), a 10x Genomics Early Career Investigator Award (D.G.), a National Institute of Neurologic Disease and Stroke K99/R00 Pathway to Independence award NS112458-01A1 (D.G.), an Irene Diamond Fund/AFAR Postdoctoral Transition Award in Aging (D.G.), the Cure Alzheimer's Fund (D.G.), the Alzheimer's Association ADSF-21-818117 (D.G. and T.W.-C.), the NOMIS Foundation (T.W.-C.), NIA R01AG045034 05 (T.W.-C.), the NIA funded Stanford ADRC P50AG047366 and P30AG066515 (V.W.H.), R01AG048076 (A.D.W.), UC San Diego Shiley-Marcos ADRC P30 AG062429 (D.R.G.), and a pilot project through the Northwestern University ADRC 1P30AG072977-01 (D.G.).

AUTHOR CONTRIBUTIONS

N.P. performed bioinformatics analysis and generated figures. L.v.O. directed experiments, edited figures, and conducted confocal imaging. A.R., V.T., B.S., Z.Z., E.T., and D.C. assisted with sample processing. E.T. and D.G. performed cell sorting and library preparation. H.O., P.M.L., and J.R. assisted with CSF protein measurements and analysis. F.E., D.R.G., A.N.T., E.C.M., V.W.H., and A.D.W. provided patient samples. T.W.-C. provided reagents. D.G. conceptualized and led the study and wrote the manuscript. All authors read and approved the final manuscript.

DECLARATION OF INTERESTS

T.W.-C. and D.G. are co-inventors on a patent related to this work. Patent US-2022-0170908-A1 is for compositions and methods for measuring T cell markers associated with AD.

Received: June 21, 2022
Revised: September 27, 2022
Accepted: November 17, 2022
Published: December 13, 2022

REFERENCES

1. Wyss-Coray, T., and Mucke, L. (2002). Inflammation in neurodegenerative disease–a double-edged sword. Neuron *35*, 419–432. https://doi.org/10.1016/s0896-6273(02)00794-8.
2. Aspelund, A., Antila, S., Proulx, S.T., Karlsen, T.V., Karaman, S., Detmar, M., Wiig, H., and Alitalo, K. (2015). A dural lymphatic vascular system that drains brain interstitial fluid and macromolecules. J. Exp. Med. *212*, 991–999. https://doi.org/10.1084/jem.20142290.
3. Louveau, A., Smirnov, I., Keyes, T.J., Eccles, J.D., Rouhani, S.J., Peske, J.D., Derecki, N.C., Castle, D., Mandell, J.W., Lee, K.S., et al. (2015). Structural and functional features of central nervous system lymphatic vessels. Nature *523*, 337–341. https://doi.org/10.1038/nature14432.
4. Bartholomäus, I., Kawakami, N., Odoardi, F., Schläger, C., Miljkovic, D., Ellwart, J.W., Klinkert, W.E., Flügel-Koch, C., Issekutz, T.B., Wekerle, H., and Flugel, A. (2009). Effector T cell interactions with meningeal vascular structures in nascent autoimmune CNS lesions. Nature *462*, 94–98. https://doi.org/10.1038/nature08478.
5. Kivisäkk, P., Mahad, D.J., Callahan, M.K., Trebst, C., Tucky, B., Wei, T., Wu, L., Baekkevold, E.S., Lassmann, H., Staugaitis, S.M., et al. (2003). Human cerebrospinal fluid central memory CD4+ T cells: evidence for trafficking through choroid plexus and meninges via P-selectin. Proc. Natl. Acad. Sci. USA *100*, 8389–8394. https://doi.org/10.1073/pnas.1433000100.
6. Reboldi, A., Coisne, C., Baumjohann, D., Benvenuto, F., Bottinelli, D., Lira, S., Uccelli, A., Lanzavecchia, A., Engelhardt, B., and Sallusto, F. (2009). C-C chemokine receptor 6-regulated entry of TH-17 cells into the CNS through the choroid plexus is required for the initiation of EAE. Nat. Immunol. *10*, 514–523. https://doi.org/10.1038/ni.1716.
7. Schläger, C., Körner, H., Krueger, M., Vidoli, S., Haberl, M., Mielke, D., Brylla, E., Issekutz, T., Cabañas, C., Nelson, P.J., et al. (2016). Effector T-cell trafficking between the leptomeninges and the cerebrospinal fluid. Nature *530*, 349–353. https://doi.org/10.1038/nature16939.
8. Baruch, K., Deczkowska, A., David, E., Castellano, J.M., Miller, O., Kertser, A., Berkutzki, T., Barnett-Itzhaki, Z., Bezalel, D., Wyss-Coray, T., et al. (2014). Aging. Aging-induced type I interferon response at the choroid plexus negatively affects brain function. Science *346*, 89–93. https://doi.org/10.1126/science.1252945.
9. Schwartz, M. (2017). Can immunotherapy treat neurodegeneration? Science *357*, 254–255. https://doi.org/10.1126/science.aai8231.

10. Cugurra, A., Mamuladze, T., Rustenhoven, J., Dykstra, T., Beroshvili, G., Greenberg, Z.J., Baker, W., Papadopoulos, Z., Drieu, A., Blackburn, S., et al. (2021). Skull and vertebral bone marrow are myeloid cell reservoirs for the meninges and CNS parenchyma. Science *373*. https://doi.org/10.1126/science.abf7844.

11. Mazzitelli, J.A., Smyth, L.C.D., Cross, K.A., Dykstra, T., Sun, J., Du, S., Mamuladze, T., Smirnov, I., Rustenhoven, J., and Kipnis, J. (2022). Cerebrospinal fluid regulates skull bone marrow niches via direct access through dural channels. Nat. Neurosci. *25*, 555–560. https://doi.org/10.1038/s41593-022-01029-1.

12. Pulous, F.E., Cruz-Hernández, J.C., Yang, C., Kaya, Z., Paccalet, A., Wojtkiewicz, G., Capen, D., Brown, D., Wu, J.W., Schloss, M.J., et al. (2022). Cerebrospinal fluid can exit into the skull bone marrow and instruct cranial hematopoiesis in mice with bacterial meningitis. Nat. Neurosci. *25*, 567–576. https://doi.org/10.1038/s41593-022-01060-2.

13. Gate, D., Saligrama, N., Leventhal, O., Yang, A.C., Unger, M.S., Middeldorp, J., Chen, K., Lehallier, B., Channappa, D., De Los Santos, M.B., et al. (2020). Clonally expanded CD8 T cells patrol the cerebrospinal fluid in Alzheimer's disease. Nature *577*, 399–404. https://doi.org/10.1038/s41586-019-1895-7.

14. Gate, D., Tapp, E., Leventhal, O., Shahid, M., Nonninger, T.J., Yang, A.C., Strempfl, K., Unger, M.S., Fehlmann, T., Oh, H., et al. (2021). CD4(+) T cells contribute to neurodegeneration in Lewy body dementia. Science *374*, 868–874. https://doi.org/10.1126/science.abf7266.

15. Kowarik, M.C., Grummel, V., Wemlinger, S., Buck, D., Weber, M.S., Berthele, A., and Hemmer, B. (2014). Immune cell subtyping in the cerebrospinal fluid of patients with neurological diseases. J. Neurol. *261*, 130–143. https://doi.org/10.1007/s00415-013-7145-2.

16. Svenningsson, A., Hansson, G.K., Andersen, O., Andersson, R., Patarroyo, M., and Stemme, S. (1993). Adhesion molecule expression on cerebrospinal fluid T lymphocytes: evidence for common recruitment mechanisms in multiple sclerosis, aseptic meningitis, and normal controls. Ann. Neurol. *34*, 155–161. https://doi.org/10.1002/ana.410340210.

17. Oh, H., Leventhal, O., Channappa, D., Henderson, V.W., Wyss-Coray, T., Lehallier, B., and Gate, D. (2021). Methods to investigate intrathecal adaptive immunity in neurodegeneration. Mol. Neurodegener. *16*, 3. https://doi.org/10.1186/s13024-021-00423-w.

18. Young, M.D., and Behjati, S. (2020). SoupX removes ambient RNA contamination from droplet-based single-cell RNA sequencing data. GigaScience *9*. https://doi.org/10.1093/gigascience/giaa151.

19. Baecher-Allan, C., Wolf, E., and Hafler, D.A. (2006). MHC class II expression identifies functionally distinct human regulatory T cells. J. Immunol. *176*, 4622–4631. https://doi.org/10.4049/jimmunol.176.8.4622.

20. Saraiva, D.P., Jacinto, A., Borralho, P., Braga, S., and Cabral, M.G. (2018). HLA-DR in cytotoxic T lymphocytes predicts breast cancer patients' response to neoadjuvant chemotherapy. Front. Immunol. *9*, 2605. https://doi.org/10.3389/fimmu.2018.02605.

21. Tippalagama, R., Singhania, A., Dubelko, P., Lindestam Arlehamn, C.S., Crinklaw, A., Pomaznoy, M., Seumois, G., deSilva, A.D., Premawansa, S., Vidanagama, D., et al. (2021). HLA-DR marks recently divided antigen-specific effector CD4 T cells in active tuberculosis patients. J. Immunol. *207*, 523–533. https://doi.org/10.4049/jimmunol.2100011.

22. Viallard, J.F., Bloch-Michel, C., Neau-Cransac, M., Taupin, J.L., Garrigue, S., Miossec, V., Mercie, P., Pellegrin, J.L., and Moreau, J.F. (2001). HLA-DR expression on lymphocyte subsets as a marker of disease activity in patients with systemic lupus erythematosus. Clin. Exp. Immunol. *125*, 485–491. https://doi.org/10.1046/j.1365-2249.2001.01623.x.

23. Peters, P.J., Borst, J., Oorschot, V., Fukuda, M., Krähenbühl, O., Tschopp, J., Slot, J.W., and Geuze, H.J. (1991). Cytotoxic T lymphocyte granules are secretory lysosomes, containing both perforin and granzymes. J. Exp. Med. *173*, 1099–1109. https://doi.org/10.1084/jem.173.5.1099.

24. Bertram, L., McQueen, M.B., Mullin, K., Blacker, D., and Tanzi, R.E. (2007). Systematic meta-analyses of Alzheimer disease genetic association studies: the AlzGene database. Nat. Genet. *39*, 17–23. https://doi.org/10.1038/ng1934.

25. Chartier-Harlin, M.C., Parfitt, M., Legrain, S., Pérez-Tur, J., Brousseau, T., Evans, A., Berr, C., Vidal, O., Roques, P., and Gourlet, V. (1994). Apolipoprotein E, epsilon 4 allele as a major risk factor for sporadic early and late-onset forms of Alzheimer's disease: analysis of the 19q13.2 chromosomal region. Hum. Mol. Genet. *3*, 569–574. https://doi.org/10.1093/hmg/3.4.569.

26. Drigalenko, E., Poduslo, S., and Elston, R. (1998). Interaction of the apolipoprotein E and CI loci in predisposing to late-onset Alzheimer's disease. Neurology *51*, 131–135. https://doi.org/10.1212/wnl.51.1.131.

27. Farrer, L.A., Cupples, L.A., Haines, J.L., Hyman, B., Kukull, W.A., Mayeux, R., Myers, R.H., Pericak-Vance, M.A., Risch, N., and van Duijn, C.M. (1997). Effects of age, sex, and ethnicity on the association between apolipoprotein E genotype and Alzheimer disease. A meta-analysis. APOE and Alzheimer disease meta analysis consortium. JAMA *278*, 1349–1356.

28. Ki, C.S., Na, D.L., Kim, D.K., Kim, H.J., and Kim, J.W. (2002). Genetic association of an apolipoprotein C-I (APOC1) gene polymorphism with late-onset Alzheimer's disease. Neurosci. Lett. *319*, 75–78. https://doi.org/10.1016/s0304-3940(01)02559-9.

29. Kuerban, B., Shibata, N., Komatsu, M., Ohnuma, T., and Arai, H. (2010). Genetic association between PLTP gene polymorphisms and Alzheimer's disease in a Japanese population. Dement. Geriatr. Cogn. Disord. *30*, 78–82. https://doi.org/10.1159/000318855.

30. Tycko, B., Lee, J.H., Ciappa, A., Saxena, A., Li, C.M., Feng, L., Arriaga, A., Stern, Y., Lantigua, R., Shachter, N., and Mayeux, R. (2004). APOE and APOC1 promoter polymorphisms and the risk of Alzheimer disease in African American and Caribbean Hispanic individuals. Arch. Neurol. *61*, 1434–1439. https://doi.org/10.1001/archneur.61.9.1434.

31. Desrumaux, C., Lemaire-Ewing, S., Ogier, N., Yessoufou, A., Hammann, A., Sequeira-Le Grand, A., Deckert, V., Pais de Barros, J.P., Le Guern, N., Guy, J., et al. (2016). Plasma phospholipid transfer protein (PLTP) modulates adaptive immune functions through alternation of T helper cell polarization. Cell. Mol. Immunol. *13*, 795–804. https://doi.org/10.1038/cmi.2015.75.

32. Finak, G., McDavid, A., Yajima, M., Deng, J., Gersuk, V., Shalek, A.K., Slichter, C.K., Miller, H.W., McElrath, M.J., Prlic, M., et al. (2015). MAST: a flexible statistical framework for assessing transcriptional changes and characterizing heterogeneity in single-cell RNA sequencing data. Genome Biol. *16*, 278. https://doi.org/10.1186/s13059-015-0844-5.

33. Lehallier, B., Gate, D., Schaum, N., Nanasi, T., Lee, S.E., Yousef, H., Moran Losada, P., Berdnik, D., Keller, A., Verghese, J., et al. (2019). Undulating changes in human plasma proteome profiles across the lifespan. Nat. Med. *25*, 1843–1850. https://doi.org/10.1038/s41591-019-0673-2.

34. Perry, D.C., Lehmann, M., Yokoyama, J.S., Karydas, A., Lee, J.J., Coppola, G., Grinberg, L.T., Geschwind, D., Seeley, W.W., Miller, B.L., et al. (2013). Progranulin mutations as risk factors for Alzheimer disease. JAMA Neurol. *70*, 774–778. https://doi.org/10.1001/2013.jamaneurol.393.

35. Goedert, M., and Spillantini, M.G. (2006). Frontotemporal lobar degeneration through loss of progranulin function. Brain *129*, 2808–2810. https://doi.org/10.1093/brain/awl291.

36. Le Ber, I., van der Zee, J., Hannequin, D., Gijselinck, I., Campion, D., Puel, M., Laquerrière, A., De Pooter, T., Camuzat, A., Van den Broeck, M., et al. (2007). Progranulin null mutations in both sporadic and familial frontotemporal dementia. Hum. Mutat. *28*, 846–855. https://doi.org/10.1002/humu.20520.

37. Rademakers, R., Baker, M., Gass, J., Adamson, J., Huey, E.D., Momeni, P., Spina, S., Coppola, G., Karydas, A.M., Stewart, H., et al. (2007). Phenotypic variability associated with progranulin haploinsufficiency in patients with the common 1477C–>T (Arg493X) mutation: an international initiative. Lancet Neurol. *6*, 857–868. https://doi.org/10.1016/S1474-4422(07)70221-1.

38. Tanaka, Y., Chambers, J.K., Matsuwaki, T., Yamanouchi, K., and Nishihara, M. (2014). Possible involvement of lysosomal dysfunction in

pathological changes of the brain in aged progranulin-deficient mice. Acta Neuropathol. Commun. *2*, 78. https://doi.org/10.1186/s40478-014-0078-x.

39. Marschallinger, J., Iram, T., Zardeneta, M., Lee, S.E., Lehallier, B., Haney, M.S., Pluvinage, J.V., Mathur, V., Hahn, O., Morgens, D.W., et al. (2020). Lipid-droplet-accumulating microglia represent a dysfunctional and proinflammatory state in the aging brain. Nat. Neurosci. *23*, 194–208. https://doi.org/10.1038/s41593-019-0566-1.

40. Jin, S., Guerrero-Juarez, C.F., Zhang, L., Chang, I., Ramos, R., Kuan, C.H., Myung, P., Plikus, M.V., and Nie, Q. (2021). Inference and analysis of cell-cell communication using CellChat. Nat. Commun. *12*, 1088. https://doi.org/10.1038/s41467-021-21246-9.

41. Kim, C.H., Kunkel, E.J., Boisvert, J., Johnston, B., Campbell, J.J., Genovese, M.C., Greenberg, H.B., and Butcher, E.C. (2001). Bonzo/CXCR6 expression defines type 1-polarized T-cell subsets with extralymphoid tissue homing potential. J. Clin. Invest. *107*, 595–601. https://doi.org/10.1172/JCI11902.

42. Sariyar, M., and Borg, A. (2010). The RecordLinkage package: detecting errors in data. R J. *2*, 61.

43. Hao, Y., Hao, S., Andersen-Nissen, E., Mauck, W.M., 3rd, Zheng, S., Butler, A., Lee, M.J., Wilk, A.J., Darby, C., Zager, M., et al. (2021). Integrated analysis of multimodal single-cell data. Cell *184*, 3573–3587.e29. https://doi.org/10.1016/j.cell.2021.04.048.

44. Preische, O., Schultz, S.A., Apel, A., Kuhle, J., Kaeser, S.A., Barro, C., Gräber, S., Kuder-Buletta, E., LaFougere, C., Laske, C., et al. (2019). Serum neurofilament dynamics predicts neurodegeneration and clinical progression in presymptomatic Alzheimer's disease. Nat. Med. *25*, 277–283. https://doi.org/10.1038/s41591-018-0304-3.

45. Zhang, Y., Sloan, S.A., Clarke, L.E., Caneda, C., Plaza, C.A., Blumenthal, P.D., Vogel, H., Steinberg, G.K., Edwards, M.S., Li, G., et al. (2016). Purification and characterization of progenitor and mature human astrocytes reveals transcriptional and functional differences with mouse. Neuron *89*, 37–53. https://doi.org/10.1016/j.neuron.2015.11.013.

46. Gosselin, D., Skola, D., Coufal, N.G., Holtman, I.R., Schlachetzki, J.C.M., Sajti, E., Jaeger, B.N., O'Connor, C., Fitzpatrick, C., Pasillas, M.P., et al. (2017). An environment-dependent transcriptional network specifies human microglia identity. Science *356*, eaal3222. https://doi.org/10.1126/science.aal3222.

47. Webster, J.A., Gibbs, J.R., Clarke, J., Ray, M., Zhang, W., Holmans, P., Rohrer, K., Zhao, A., Marlowe, L., Kaleem, M., et al. (2009). Genetic control of human brain transcript expression in Alzheimer disease. Am. J. Hum. Genet. *84*, 445–458. https://doi.org/10.1016/j.ajhg.2009.03.011.

48. Jansen, I.E., Savage, J.E., Watanabe, K., Bryois, J., Williams, D.M., Steinberg, S., Sealock, J., Karlsson, I.K., Hägg, S., Athanasiu, L., et al. (2019). Genome-wide meta-analysis identifies new loci and functional pathways influencing Alzheimer's disease risk. Nat. Genet. *51*, 404–413. https://doi.org/10.1038/s41588-018-0311-9.

49. Kunkle, B.W., Grenier-Boley, B., Sims, R., Bis, J.C., Damotte, V., Naj, A.C., Boland, A., Vronskaya, M., van der Lee, S.J., Amlie-Wolf, A., et al. (2019). Genetic meta-analysis of diagnosed Alzheimer's disease identifies new risk loci and implicates Abeta, tau, immunity and lipid processing. Nat. Genet. *51*, 414–430. https://doi.org/10.1038/s41588-019-0358-2.

50. Yang, A.C., Vest, R.T., Kern, F., Lee, D.P., Agam, M., Maat, C.A., Losada, P.M., Chen, M.B., Schaum, N., Khoury, N., et al. (2022). A human brain vascular atlas reveals diverse mediators of Alzheimer's risk. Nature *603*, 885–892. https://doi.org/10.1038/s41586-021-04369-3.

51. Mahley, R.W. (1988). Apolipoprotein E: cholesterol transport protein with expanding role in cell biology. Science *240*, 622–630. https://doi.org/10.1126/science.3283935.

52. Shimaoka, T., Kume, N., Minami, M., Hayashida, K., Kataoka, H., Kita, T., and Yonehara, S. (2000). Molecular cloning of a novel scavenger receptor for oxidized low density lipoprotein, SR-PSOX, on macrophages. J. Biol. Chem. *275*, 40663–40666. https://doi.org/10.1074/jbc.C000761200.

53. Rosen, S.F., Soung, A.L., Yang, W., Ai, S., Kanmogne, M., Davé, V.A., Artyomov, M., Magee, J.A., and Klein, R.S. (2022). Single-cell RNA transcriptome analysis of CNS immune cells reveals CXCL16/CXCR6 as maintenance factors for tissue-resident T cells that drive synapse elimination. Genome Med. *14*, 108. https://doi.org/10.1186/s13073-022-01111-0.

54. McGinnis, C.S., Murrow, L.M., and Gartner, Z.J. (2019). DoubletFinder: doublet detection in single-cell RNA sequencing data using artificial nearest neighbors. Cell Syst. *8*, 329–337.e4. https://doi.org/10.1016/j.cels.2019.03.003.

55. Trelle, A.N., Carr, V.A., Guerin, S.A., Thieu, M.K., Jayakumar, M., Guo, W., Nadiadwala, A., Corso, N.K., Hunt, M.P., Litovsky, C.P., et al. (2020). Hippocampal and cortical mechanisms at retrieval explain variability in episodic remembering in older adults. eLife *9*, e55335. https://doi.org/10.7554/eLife.55335.

56. Trelle, A.N., Carr, V.A., Wilson, E.N., Swarovski, M.S., Hunt, M.P., Toueg, T.N., Tran, T.T., Channappa, D., Corso, N.K., Thieu, M.K., et al. (2021). Association of CSF biomarkers with hippocampal-dependent memory in preclinical Alzheimer disease. Neurology *96*. e1470–e1481. https://doi.org/10.1212/WNL.0000000000011477.

STAR★METHODS

KEY RESOURCES TABLE

REAGENT or RESOURCE	SOURCE	IDENTIFIER
Antibodies		
Rat monoclonal anti-CD3	Abcam	ab11089; RRID: AB_2889189
Rabbit monoclonal anti-CXCR6	Abcam	ab273116; RRID: AB_2925220
Mouse monoclonal anti-CXCL16	Thermo Fisher	MA5-27845; RRID: AB_2735159
Rabbit monoclonal anti-amyloid-β	Cell Signalling	8243; RRID: AB_2797642
Goat polyclonal anti-Iba1	Abcam	ab48004; RRID: AB_870576
Biological samples		
Adult CSF	Stanford Aging and Memory Study (SAMS)	N/A
Adult CSF	Stanford University Alzheimer's Disease Research Center (ADRC)	N/A
Adult CSF	University of California at San Francisco ADRC	N/A
Adult CSF	University of California at San Diego ADRC	N/A
Critical commercial assays		
10x Genomics Chromium Next GEM Single Cell 5' v2 with immune profiling kit	10xGenomics	PN-1000263
Deposited data		
Raw and processed data	This study	GEO: GSE200164
Code for analysis	This study	Github: https://github.com/gatelabnw/csf_aging
ShinyCell app for interactive data analysis	This study	ShinyApps: gatelabnu.shinyapps.io/csf_aging
Software and algorithms		
Cellranger v6.0.0	10x Genomics	https://support.10xgenomics.com/single-cell-gene-expression/software/pipelines/latest/what-is-cell-ranger
SoupX v1.5.2	Young and Behjati[18]	https://github.com/constantAmateur/SoupX
DoubletFinder v2.0.3	McGinnis et al.[54]	https://github.com/chris-mcginnis-ucsf/DoubletFinder
Seurat v4.1.0	Hao et al.[42]	https://satijalab.org/seurat/
DEswan v0.0.0.9001	Lehallier et al.[33]	https://github.com/lehallib/DEswan
CellChat v1.4.0	Jin et al.[40]	http://www.cellchat.org
RecordLinkage v0.4-12.3	Sariyar and Borg[42]	https://cran.r-project.org/web/packages/RecordLinkage/index.html

RESOURCE AVAILABILITY

Lead Contact

Further information and requests for resources should be directed to and will be fulfilled by the lead contact, David Gate (dgate@northwestern.edu).

Materials Availability

No new unique reagents were generated for this study.

Data and Code Availability

- All raw data used in this study can be found on GEO: GSE200164. Raw count and log-normalized expression matrices are also available under the same accession number.

- All code used to generate the figures in this study can be found at https://github.com/gatelabnw/csf_aging.
- Any additional information required to reanalyze the data reported in this work is available from the lead contact upon request.

EXPERIMENTAL MODEL AND SUBJECT DETAILS

Human Subjects

For scRNAseq experiments, CSF samples were acquired through the Stanford Aging and Memory Study (SAMS), Stanford University Alzheimer's Disease Research Center (ADRC), the University of California at San Francisco ADRC and the University of California at San Diego ADRC. Collection of CSF was approved by the Institutional Review Board of each university and written consent was obtained from all subjects. scRNAseq and scTCRseq were performed on CSF of 59 subjects of both sexes aged 47-82 years. Of these subjects, 45 were assessed as healthy controls while the remaining 14 were patients with cognitive impairment (MCI or dementia due to AD). Age and sex demographics are presented in Figures S1A and S1B. SAMS eligibility included normal or corrected-to-normal vision/hearing, native English speaking, no history of neurologic or psychiatric disease, a Clinical Dementia Rating (CDR) global score of zero, and performance within the normal range on a standardized neuropsychological test battery.[55,56] In the ADRCs, all healthy control participants had CDR scores of zero and were deemed cognitively unimpaired during a clinical consensus meeting consisting of neurologists, neuropsychologists, and research coordinators. All healthy control and cognitively impaired study subjects underwent neurological examinations, CDR ratings, and standardized neuropsychological assessments to determine cognitive and diagnostic status, including procedures of the National Alzheimer's Coordinating Center. All cognitively impaired participants had a CDR score greater than zero. For histology experiments, de-identified human dorsolateral prefrontal cortex samples from AD subjects of various ages were obtained through collaboration with the Stanford University ADRC.

METHOD DETAILS

Sample Preparation

CSF was collected via lumbar puncture and cells were cryopreserved according to our established protocol.[17] All 59 CSF samples were processed and cryopreserved by the same technician over the course of two years. Cells were sorted by FACS for live singlets using Sytox blue live/dead dye before performing droplet-based scRNAseq and scTCRseq.

Protein biomarker measurements

We measured protein biomarkers in CSF with two separate methods. We used PEA technology (Olink Proteomics) to measure CXCL16 and NEFL as in Figures 4I and 4J. Protein levels are presented in Normalized Protein eXpression (NPX) units. NPX is Olink's arbitrary unit, which is in Log_2 scale. NPX is calculated from Ct values and data pre-processing (normalization) is performed to minimize both intra- and inter-assay variation. Separately, we used single molecule array (Simoa) ELISA technology (Quanterix) to measure NEFL, $A\beta_{42}$ and $A\beta_{40}$, as in Figure 4J. We also measured CXCL16 and NEFL using SOMAmer technology (SomaLogic), as in Figure 4K.

Droplet-based scRNA and TCRseq

The 10x Genomics Chromium Next GEM Single Cell 5' v2 with immune profiling kit was used for scRNA and TCRseq of CSF samples. Libraries were prepared according to 10x Genomics protocols. Libraries were sequenced by Novogene on an Illumina Novaseq 6000 instrument. Bases were called using the Illumina RTA3 method. RNA reads were aligned to the hg38 genome build and gene expression matrices were generated using Cell Ranger 6.0.0 software. TCR reads were also aligned to the hg38 genome build and clonotype/contig matrices were generated using Cell Ranger.

scRNA and TCRseq quality control

Empty droplets were removed via Cell Ranger 6.0.0 using the EmptyDrops method per 10x Genomics' protocol. Gene expression matrices were corrected for background contamination using R package SoupX 1.5.2. Known monocyte/dendritic markers (CD14, CD68, MS4A7, and CD16) were used to estimate the contamination fraction of each sample. Counts were adjusted using the SoupX subtraction method using the calculated contamination fraction on a per-sample basis. Doublets were removed using R package DoubletFinder 2.0.3[54] using an approximate doublet formation rate of 1% which is consistent with the expected multiplet rate according to 10x Genomics Single Cell 5' v2 kit protocol. Any cells with fewer than 200 mapped features were eliminated, as well as any features present in fewer than three cells. Any cells with greater than 10% mitochondrial reads were also eliminated. TCR clonotypes and contigs were also filtered for empty droplets using Cell Ranger 6.0.0. Only TCR sequences associated to cells annotated with a T cell identity by RNAseq were retained.

Cell type annotations

Corrected and filtered gene expression matrices were SCTransformed with Seurat 4.1.0[43] on a per sample basis and then integrated through harmonizing 'anchors' as recommended for cell type identification in Seurat documentation. Number of reads, number of

features, and percent of mitochondrial reads were regressed out in the data scaling step of SCTransform, and the top 1000 most variable features were used. Principal component analysis (PCA) was then run on the integrated assay. The first fifteen principal components (PCs) were then used to generate a shared nearest-neighbor graph which was then clustered under the Louvain algorithm with a resolution of 0.3. Uniform manifold approximation and projection (UMAP) was then performed using the first 15 PCs and 30 nearest neighbors. Canonical cell type markers were used to identify expected cell types (markers used are shown in Figure1D). Pan T cell and monocyte clusters were then isolated, and the clustering procedure was repeated to differentiate more specific cell types.

Differential expression by linear modelling

We first aimed to identify genes with linear expression changes across age. The following model was implemented:

$$Expression \sim \alpha + \beta_1 age + \beta_2 sex + \varepsilon$$

Log-normalized counts were used for expression values as recommended for differential expression analyses by the developers of Seurat. α represents the y-intercept, β values represent the associated slope with the variable of interest, and ε represents residual error. Sex was included as a covariate to account for variations in sex composition of the cohort across age. Only genes expressed in at least 10% of cells in the respective cell type were used for differential expression throughout the study. Linear models were generated using the R package stats function, *lm*. Type II sum of squares were calculated using the R package car function, *Anova*. P values were adjusted for multiple comparisons using the Benjamini-Hochberg procedure. Thresholds of 0.01 for adjusted p value and 0.005 for β were used to determine significant DEGs.

DE-SWAN analysis

DE-SWAN was implemented to identify more transient gene expression changes across age. The following model was used:

$$Expression \sim \alpha + \beta_1 I_{k\ low/high} + \varepsilon$$

$I_{k\ low/high}$ represents the binarization of age binned above and below k centers. 10 centers with windows of $\pm$ 2 years from ages 62 to 82 were used. Number of cells per age bin per cell type differed dramatically from one center to the next. To mitigate the effect of cell number on number of DEGs, we randomly sampled 200 cells with replacement from each age for each cell type. Gene counts for every twenty cells were summed to generate a 'pseudocell' and then log-normalized. Type II sum of squares were calculated using the R package car function, *Anova*. P-values were adjusted for multiple comparisons using the Benjamini-Hochberg procedure. Significant DEGs were identified with thresholds of 1e-4 for adjusted p-value and 1e-4 for β.

LOESS trajectory analysis

LOESS was employed to identify non-linear patterns of gene expression over age. We initially focused on healthy aging and thus selected cognitively normal samples only. To avoid variable cell number per sample skewing the analysis, we proceeded with pseudobulked expression values. Counts for each cell type per sample were summed and then log-normalized. Genes were filtered for expression by at least 10% of cells per cell type and expression values were scaled and centered. A LOESS regression of span 0.75 was fit to each gene using the *loess* function of the R stats package. The predicted expression trajectories over age were then subdivided into 6 and 12 groups by hierarchal clustering via *hclust* function from the R stats package. LOESS curves of average expression per age point in each cluster are also reported with their associated standard errors.

Differential expression by MAST

The Seurat function *FindMarkers* was used to identify DEGs across age and diagnosis. MAST was chosen to test significance as it employs a hurdle model specifically tailored to bimodal expression distributions often observed in scRNAseq. Only genes expressed in at least 10% of cells were tested. Sex was included as a latent variable to account for sex composition changes in the cohort across age. P values were adjusted for multiple comparisons using the Benjamini-Hochberg procedure. Genes with an adjusted p value less than 0.01 and average log-fold change magnitude greater than 0.25 were considered significantly differentially expressed.

CellChat analysis

The R package CellChat[40] was used to quantitatively infer and analyze intercellular communication networks from our scRNAseq data. CellChat uses network analysis and pattern recognition approaches to predict major signaling inputs and outputs for cells and how those cells and signals coordinate for functions. CellChat classifies signaling pathways and delineates conserved and context-specific pathways through manifold learning and quantitative contrasts. CellChat calculates the communication probability of a ligand-receptor pair between two cell types using a law of mass action model which depends on ligand and receptor concentration, any known cofactor concentrations, and the number of cells in each cell type. Significance is determined by if this communication probability is statistically higher between these known cell types than between randomly permuted groups of cells.

Levenshtein similarity network

Clonotypes with unambiguous CDR3 regions on both α and β chains and a frequency of at least 2 were retained to assess TCR similarity. Both CDR3 regions were concatenated together for each cell and Levenshtein similarity (Lsim)[42] was calculated between every

possible TCR pair within and between all samples. Lsim was calculated by first finding the minimum number of deletions, additions, or substitutions needed to change one string to another, this value being the Levenshtein distance. This distance was then divided by the maximum length of both strings and subtracted from 1 to generate the Lsim. Individuals were binned into four healthy, cognitively normal age groups of equal size and one cognitively impaired group. TCR pairs with Lsim > 0.9 were used for visualization on the network plot.

Clone expression scatterplot

We aimed to evaluate the heterogeneity of gene expression in cells of expanded or individual T cell clones in healthy versus cognitively impaired individuals. The top five most expanded clones in healthy and diseased individuals were selected. To create nonclonal bootstrap cells, fifty clones of frequency 1 were randomly selected from each diagnosis group. These 50 cells were sequestered into 5 groups and gene counts were summed then log-normalized. Average expression of all cells within an expanded clone as well as the percentage of cells in a clone/bootstrap expressing the gene of interest were calculated.

Immunohistochemistry and confocal imaging

We stained 5μm paraffin-embedded brain tissue sections using antibodies rat anti-CD3 (Abcam ab11089), rabbit anti-CXCR6 (Abcam ab273116), mouse anti-CXCL16 (Thermo MA5-27845), rabbit anti-amyloid-β (Cell Signaling 8243) and goat anti-Iba1 (Abcam ab48004). Sections were deparaffinized, then antigen retrieval was performed using citrate buffer pH 6.0 for 30 min at 98°C. Sections were blocked in phosphate-buffered saline containing 10% normal donkey serum and 0.3% triton-x. Sections were stained overnight in primary antibodies. The following morning, sections were incubated with highly cross-absorbed, species-appropriate secondary antibodies. Sections were imaged on a Nikon AXR confocal microscope with a 60x objective.

ShinyCell

ShinyCell is an R package developed to quickly generate interactive Shiny-based web applications to visualize the core analysis of scRNAseq data. We have released a modified ShinyCell app allowing users to view metadata and gene expression on a UMAP, compare gene expression between various groups via violin/box plots, and other built-in analyses. Notably, we added an additional page allowing the user to view LOESS trajectories of any gene of interest between HC and CI patients in a selected cell type as well as download the associated pseudobulk data.

QUANTIFICATION AND STATISTICAL ANALYSIS

R 4.1.1 and Prism 9.2.0 were used for all statistical analyses. Statistical methods are described in the figure legends or main text as appropriate.

CellPress
OPEN ACCESS

Supplemental figures

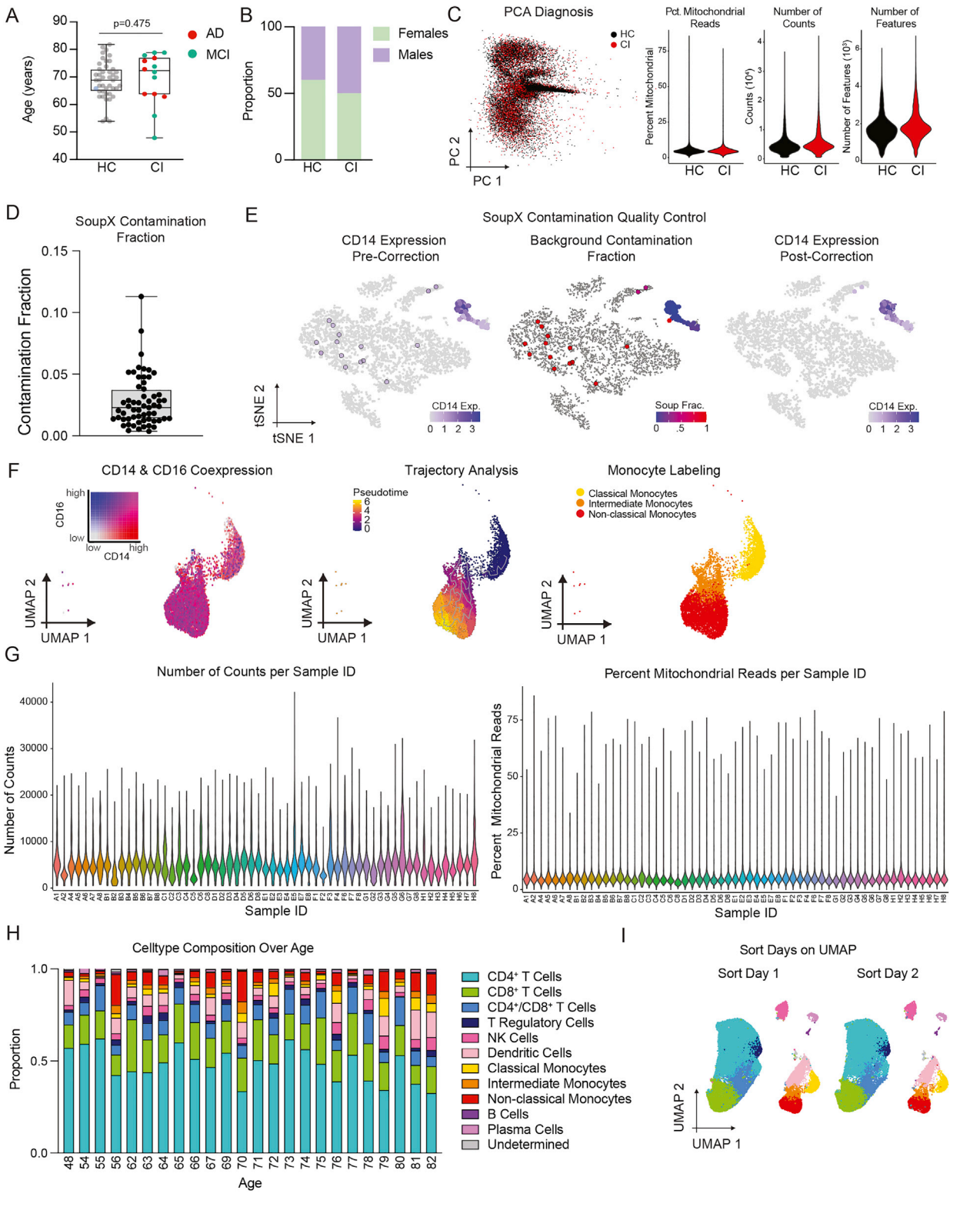

(legend on next page)

Figure S1. Quality control metrics for scRNA-seq experiments, related to Figure 1

(A) Age demographics of subjects analyzed by scRNA-seq. Mean ± SEM; Mann-Whitney U test.

(B) Sex demographics of subjects analyzed by scRNA-seq.

(C) PCA plot showing overlapping distribution of CSF cells from healthy and cognitively impaired subjects. Mitochondrial reads, counts and number of features per cell for each diagnosis are also shown.

(D) Quantification of SoupX contamination for all samples. Error bars indicate minimum and maximum.

(E) Representative SoupX quality control showing reduction of limited amounts of contaminating background CD14 RNA.

(F) Co-expression of CD14 and CD16, with accompanying cluster labels and pseudotime analysis used to distinguish classical, intermediate and nonclassical monocytes.

(G) Number of counts and mitochondrial reads per sample.

(H) Composition of cell types with age.

(I) UMAP divided by sample sort day showing lack of batch effects by processing day.

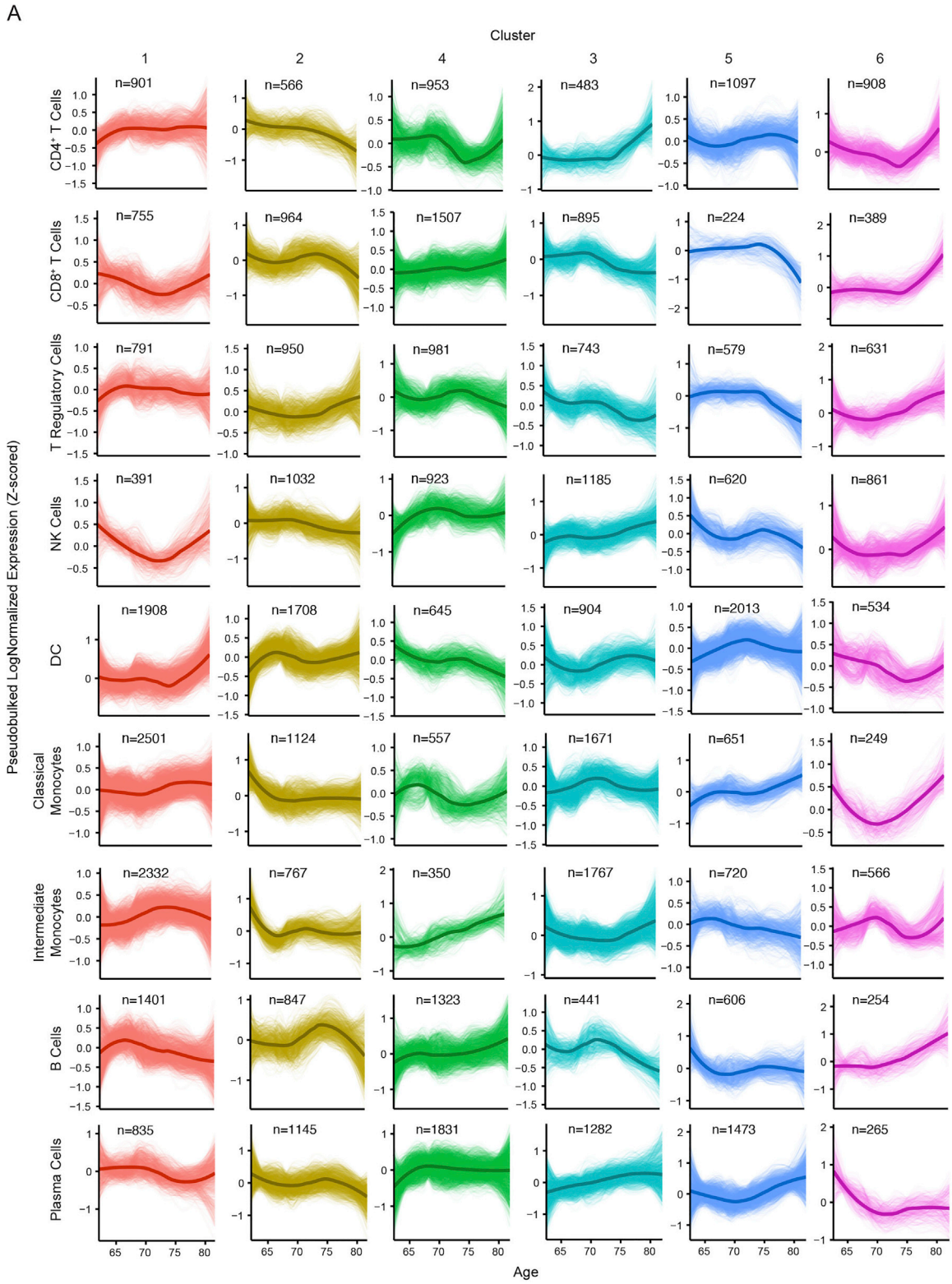

Figure S2. Distinct wave-like patterns of gene expression with age, related to Figure 2

Gene cluster trajectories plotted by LOESS. Genes expressed by at least 10% of cells for a given cell type were plotted by LOESS, then grouped into six clusters by hierarchical clustering. Patterns of gene expression with age are shown for all clusters.

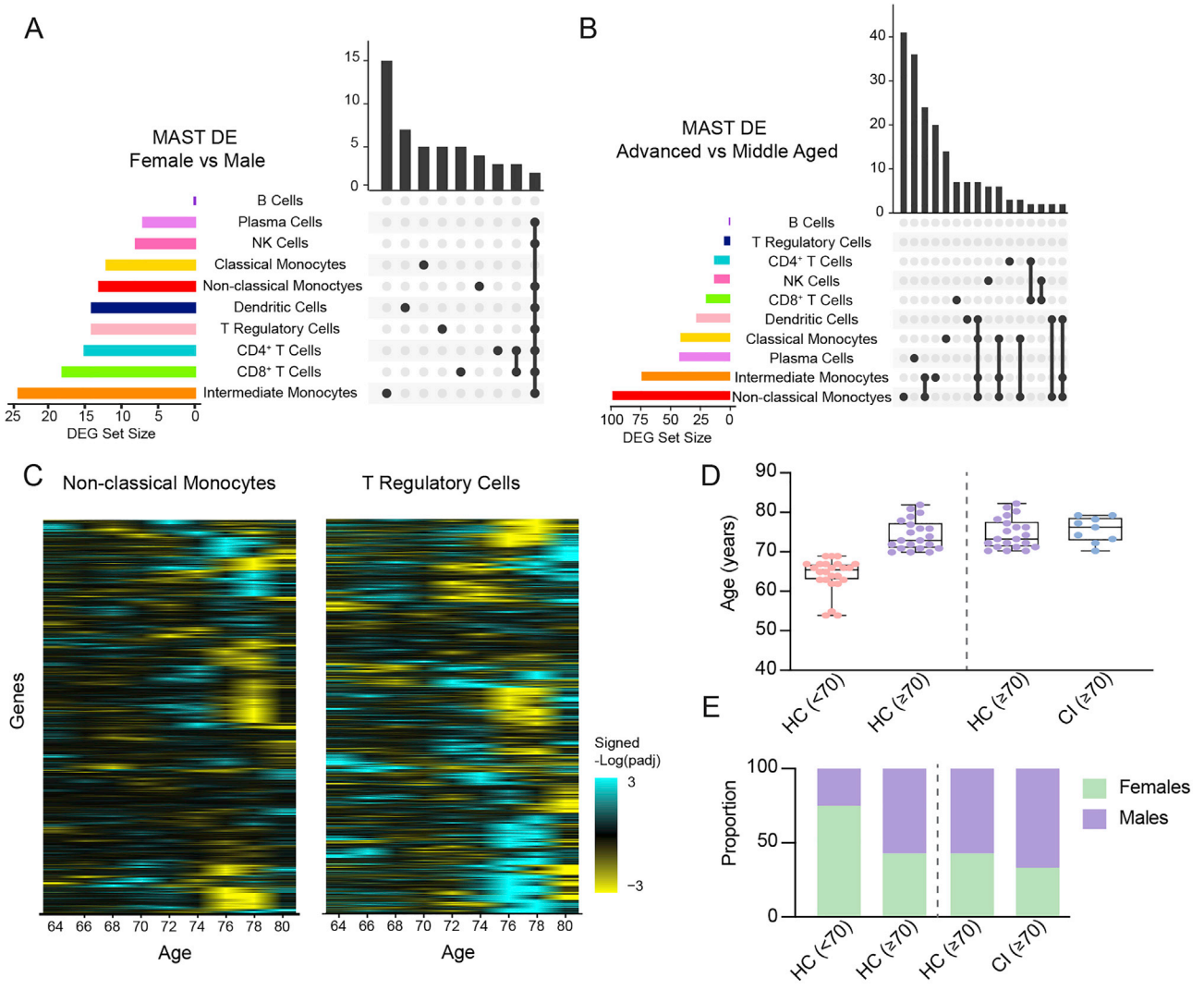

Figure S3. Non-linear gene expression changes in CSF cells with age, related to Figure 2

(A) UpSet plot showing the number of DEGs per cell cluster by MAST differential expression between female and male cognitively normal subjects.

(B) UpSet plot showing the number of DEGs per cell cluster by MAST differential expression between advanced and middle-aged cognitively normal subjects.

(C) Heatmaps showing gene expression changes with age from DE-SWAN analysis of nonclassical monocytes and Tregs.

(D and E) (D) Age and (E) sex makeup of middle-aged healthy versus advanced age healthy subjects and advanced age healthy versus advanced age cognitively impaired subjects. Error bars indicate minimum and maximum.

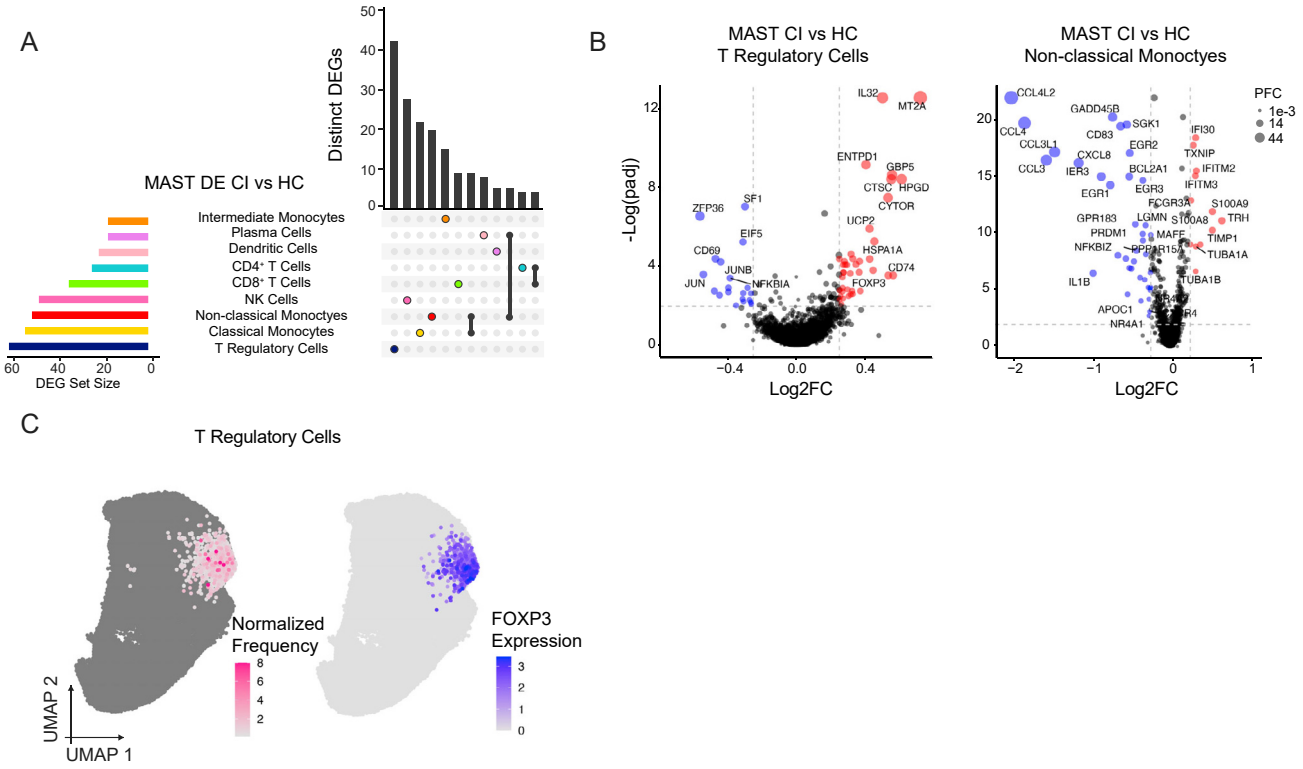

Figure S4. Immune disruption in CSF of cognitively impaired subjects, related to Figure 4

(A) MAST differential expression of cognitively impaired vs. cognitively normal controls revealed the highest level of transcriptomic dysregulation in Tregs and monocytes.

(B) Differentially expressed genes showing upregulated expression of *FOXP3* and *IL32* in Tregs. Nonclassical monocytes were also highly dysregulated. Note the downregulated expression of *APOC1* in nonclassical monocytes.

(C) UMAP distribution of *FOXP3* expression with normalized clonal T cell frequency of T regulatory cells.

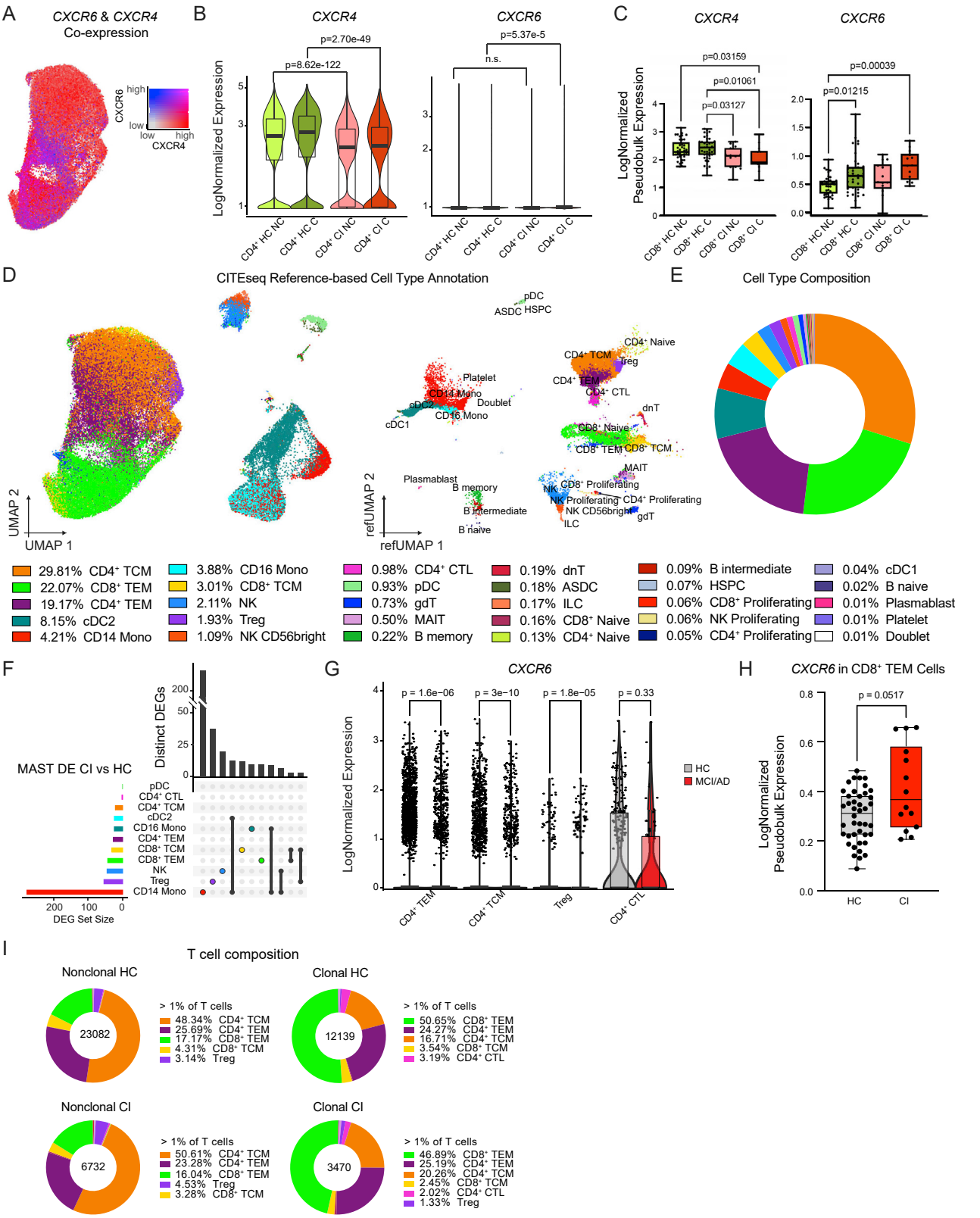

(legend on next page)

Figure S5. Clonal T cell disruption in CSF of patients with cognitive impairment, related to Figure 4

(A) UMAP plots showing the distribution of T cells expressing *CXCR6* or *CXCR4*.

(B) Single-cell quantification of *CXCR4* and *CXCR6* showing a shift down in *CXCR4* and a shift up in *CXCR6* expression in clonal T cells of cognitively impaired subjects. p values are from MAST differential expression.

(C) Pseudobulk quantification of expression of clonal and nonclonal $CD8^+$ T cells from cognitively impaired and cognitively normal CSF. p values are from one-way ANOVA.

(D) UMAP plots showing distribution of CSF cells using supervised clustering via a CITE-seq reference dataset.

(E) Donut plot showing the percentages of CSF immune cell subtypes.

(F) UpSet plot of MAST differential expression between cognitively impaired and healthy showing CD14 monocytes as most dysregulated.

(G) Single-cell *CXCR6* expression among $CD4^+$ T cells showing $CD4^+$ T_{EM} cells as the main expressors of *CXCR6*. Wilcox test, BH corrected.

(H) Pseudobulk quantification of *CXCR6* in CD8 T_{EM} T cells. t-test with Welch's correction. Error bars indicate minimum and maximum.

(I) Percentages of T cell subtypes of clonal and nonclonal CSF T cells in cognitively normal and cognitively impaired subjects.

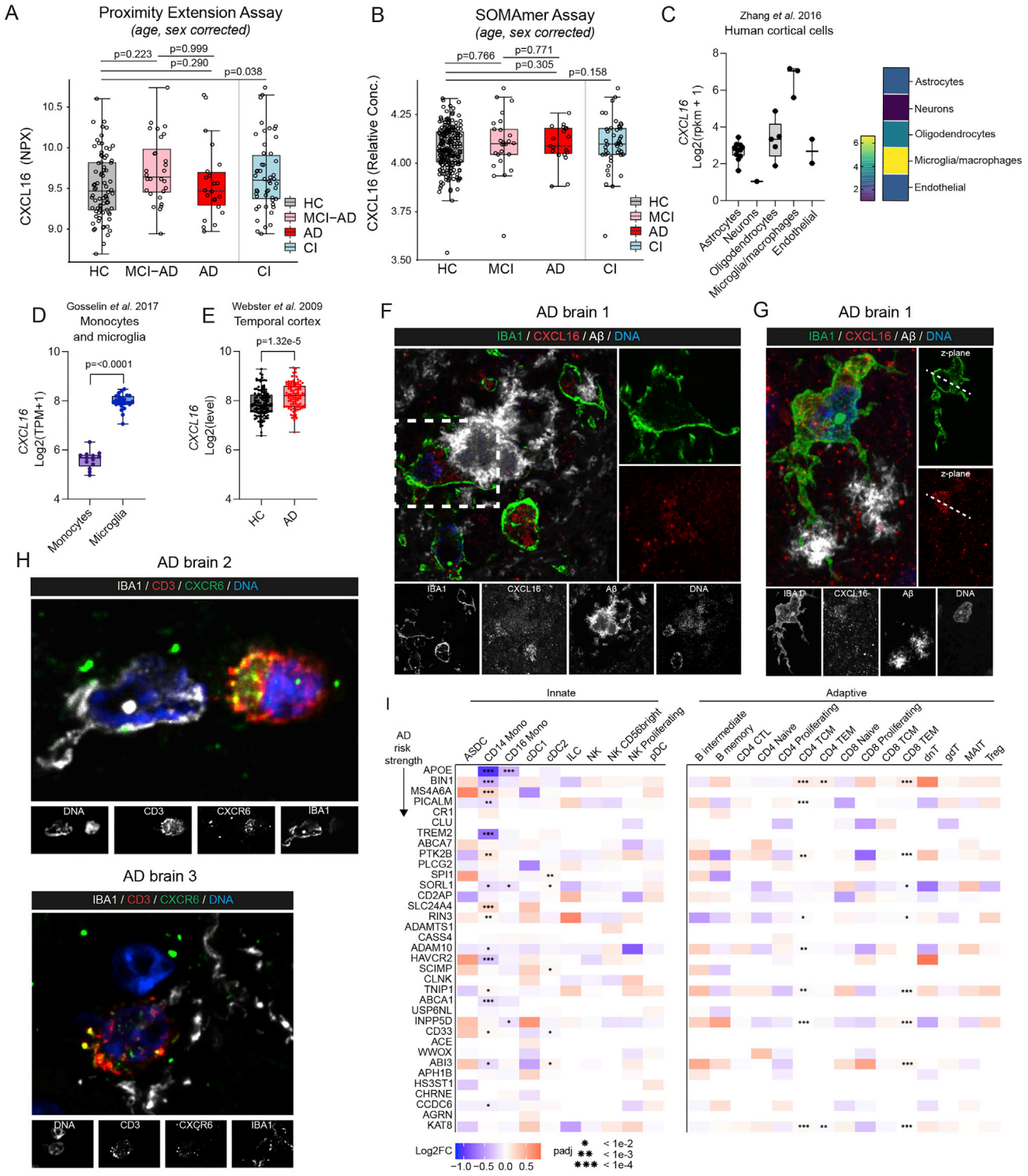

Figure S6. CXCL16-CXCR6 signaling in Alzheimer's disease, related to Figures 4 and 5

(A) Quantification of CXCL16 using proximity extension assay. p values are from ANCOVA analysis using age and sex as covariates. ANCOVA with sex and age as covariates. Error bars indicate upper and lower interquartile range (IQR) plus or minus 1.5*IQR.

(B) Quantification of CXCL16 using SOMAmer assay. p values are from ANCOVA analysis using age and sex as covariates.

(C) *CXCL16* expression among human brain cells indicates microglia/macrophages as the highest expressors. Error bars indicate minimum and maximum.

(D) Microglia express higher levels of *CXCL16* than monocytes in the brain. Unpaired t test, two-tailed. Error bars indicate minumum and maximum.

(legend continued on next page)

(E) *CXCL16* is significantly higher in AD than control temporal cortex. Unpaired t test, two-tailed. Error bars indicate minumum and maximum.
(F) Iba1$^+$ myeloid cells expressing CXCL16 adjacent to an amyloid-β plaque.
(G) Confocal z stack demonstrating intracellular expression of CXCL16 in an Iba1$^+$ myeloid cell adjacent to an amyloid-β plaque.
(H) CD3$^+$ T cells expressing CXCR6 adjacent to Iba1$^+$ myeloid cells in two separate AD post-mortem brains.
(I) Differential expression of the top 45 AD GWAS genes across all supervised CSF immune cell types. Asterisks denote the most highly altered genes by adjusted p value. Note that subsets of T cells differentially express numerous AD risk genes in CI CSF.